The Chicxulub Asteroid Impact and Mass Extinction at the Cretaceous-Paleogene Boundary

Peter Schulte,[1]* Laia Alegret,[2] Ignacio Arenillas,[2] José A. Arz,[2] Penny J. Barton,[3] Paul R. Bown,[4] Timothy J. Bralower,[5] Gail L. Christeson,[6] Philippe Claeys,[7] Charles S. Cockell,[8] Gareth S. Collins,[9] Alexander Deutsch,[10] Tamara J. Goldin,[11] Kazuhisa Goto,[12] José M. Grajales-Nishimura,[13] Richard A. F. Grieve,[14] Sean P. S. Gulick,[6] Kirk R. Johnson,[15] Wolfgang Kiessling,[16] Christian Koeberl,[11] David A. Kring,[17] Kenneth G. MacLeod,[18] Takafumi Matsui,[19] Jay Melosh,[20] Alessandro Montanari,[21] Joanna V. Morgan,[9] Clive R. Neal,[22] Douglas J. Nichols,[15] Richard D. Norris,[23] Elisabetta Pierazzo,[24] Greg Ravizza,[25] Mario Rebolledo-Vieyra,[26] Wolf Uwe Reimold,[16] Eric Robin,[27] Tobias Salge,[28] Robert P. Speijer,[29] Arthur R. Sweet,[30] Jaime Urrutia-Fucugauchi,[31] Vivi Vajda,[32] Michael T. Whalen,[33] Pi S. Willumsen[32]

The Cretaceous-Paleogene boundary ~65.5 million years ago marks one of the three largest mass extinctions in the past 500 million years. The extinction event coincided with a large asteroid impact at Chicxulub, Mexico, and occurred within the time of Deccan flood basalt volcanism in India. Here, we synthesize records of the global stratigraphy across this boundary to assess the proposed causes of the mass extinction. Notably, a single ejecta-rich deposit compositionally linked to the Chicxulub impact is globally distributed at the Cretaceous-Paleogene boundary. The temporal match between the ejecta layer and the onset of the extinctions and the agreement of ecological patterns in the fossil record with modeled environmental perturbations (for example, darkness and cooling) lead us to conclude that the Chicxulub impact triggered the mass extinction.

Paleontologists have long recognized the global scale and abruptness of the major biotic turnover at the Cretaceous-Paleogene (K-Pg, formerly K-T) boundary ~65.5 million years ago (Ma). This boundary represents one of the most devastating events in the history of life (1) and abruptly ended the age of the dinosaurs. Thirty years ago, the discovery of an anomalously high abundance of iridium and other platinum group elements (PGEs) in the K-Pg boundary clay led to the hypothesis that an asteroid ~10 km in diameter collided with Earth and rendered many environments uninhabitable (2, 3).

The occurrence of an impact is substantiated by the recognition of impact ejecta including spherules, shocked minerals, and Ni-rich spinels in many K-Pg boundary event deposits [e.g., (4, 5)]. The ejecta distribution points to an impact event in the Gulf of Mexico–Caribbean region; this prediction is reinforced by the discovery of the ~180- to 200-km-diameter Chicxulub crater structure on the Yucatan peninsula, Mexico (6). Modeling suggests that the size of the crater and the release of climatically sensitive gases from the carbonate- and sulfate-rich target rocks could have caused catastrophic environmental effects such as extended darkness, global cooling, and acid rain (7–9). These effects provide an array of potential mechanisms for the ecologically diverse but selective abrupt extinctions (Fig. 1) (10–13).

Notwithstanding the substantial evidence supporting an impact mechanism, other interpretations of the K-Pg boundary mass extinction remain. Stratigraphic and micropaleontological data from the Gulf of Mexico and the Chicxulub crater have instead been used to argue that this impact preceded the K-Pg boundary by several hundred thousand years and therefore could not have caused the mass extinction [e.g., (14)]. In addition, the approximately one-million-year-long emplacement of the large Deccan flood basalts in India spans the K-Pg boundary (Fig. 1); the release of sulfur and carbon dioxide during these voluminous eruptions may have caused severe environmental effects (15) that have also been proposed as triggers for the mass extinction at the K-Pg boundary (16).

Here, we assess the observational support for these divergent interpretations by synthesizing recent stratigraphic, micropaleontological, petrological, and geochemical data from the globally distributed K-Pg boundary event deposit. Impact and volcanism as extinction mechanisms are evaluated in terms of their predicted environmental perturbations and, ultimately, the distribution of life on Earth before and after the K-Pg boundary.

## What Is the Evidence for Correlating the Impact with the K-Pg Boundary?

The Upper Cretaceous and lower Paleogene sediments bracketing the K-Pg boundary event deposits are among the most intensively investigated deposits in the geological record. More than 350 K-Pg boundary sites are currently known, and these sites show a distinct ejecta distribution pattern related to distance from the Chicxulub crater (Fig. 2 and table

[1]GeoZentrum Nordbayern, Universität Erlangen-Nürnberg, Schlossgarten 5, D-91054 Erlangen, Germany. [2]Departamento de Ciencias de la Tierra e Instituto Universitario de Investigación de Ciencias Ambientales de Aragón, Universidad de Zaragoza, Pedro Cerbuna 12, E-50009 Zaragoza, Spain. [3]Department of Earth Sciences, University of Cambridge, Cambridge CB2 3EQ, UK. [4]Department of Earth Sciences, University College London, Gower Street, London WC1E 6BT, UK. [5]Department of Geosciences, Pennsylvania State University, University Park, PA 16802, USA. [6]Institute for Geophysics, Jackson School of Geosciences, University of Texas at Austin, J.J. Pickle Research Campus, 10100 Burnet Road 196-ROC, Austin, TX 78759, USA. [7]Earth System Science, Vrije Universiteit Brussel, Pleinlaan 2, B-1050 Brussels, Belgium. [8]Centre for Earth, Planetary, Space and Astronomical Research, Open University, Milton Keynes MK7 6AA, UK. [9]Earth Science and Engineering, Imperial College London, London SW7 2BP, UK. [10]Institut für Planetologie, Universität Münster, D-48149 Münster, Germany. [11]Department of Lithospheric Research, University of Vienna, Althanstrasse 14, A-1090 Vienna, Austria. [12]Tsunami Engineering Laboratory, Disaster Control Research Center, Graduate School of Engineering, Tohoku University, 6-6-11-1106 Aoba, Aramaki, Sendai 980-8579, Japan. [13]Programa de Geología de Exploracíon y Explotacíon, Dirección de Investigación y Posgrado, Instituto Mexicano del Petróleo, Eje Lázaro Cárdenas No. 152, C.P. 07730, México City, México. [14]Earth Sciences Sector, Natural Resources Canada, Ottawa, Ontario K1A 0E4, Canada. [15]Research and Collections Division, Denver Museum of Nature and Science, 2001 Colorado Boulevard, Denver, CO 80205, USA. [16]Museum für Naturkunde, Leibniz Institute at the Humboldt University Berlin, Invalidenstrasse 43, D-10115 Berlin, Germany. [17]Center for Lunar Science and Exploration, Universities Space Research Association–Lunar and Planetary Institute, 3600 Bay Area Boulevard, Houston, TX 77058–1113, USA. [18]Department of Geological Sciences, University of Missouri, Columbia, MO 65211, USA. [19]Planetary Exploration Research Center, Chiba Institute of Technology, 2-17-1 Tsudanuma, Narashino, Chiba 275-0016, Japan. [20]Earth and Atmospheric Sciences, Purdue University, 550 Stadium Mall Drive, West Lafayette, IN 47907–2051, USA. [21]Osservatorio Geologico di Coldigioco, 62021 Apiro (MC), Italy. [22]Department of Civil Engineering and Geological Sciences, 156 Fitzpatrick Hall, University of Notre Dame, Notre Dame, IN 46556, USA. [23]SIO Geological Collections, 301 Vaughan Hall, MS-0244, Scripps Institution of Oceanography, La Jolla, CA 92093–0244, USA. [24]Planetary Science Institute, 1700 East Fort Lowell Road, Suite 106, Tucson, AZ 85719, USA. [25]Department of Geology and Geophysics, School of Ocean and Earth Science and Technology, University of Hawaii, Manoa, Honolulu, HI 96822, USA. [26]Unidad de Ciencias del Agua, Centro de Investigación Científica de Yucatán, A.C., Calle 8, No. 39, Mz. 29, S.M. 64, Cancún, Quintana Roo, 77500, México. [27]Laboratoire des Sciences du Climat et de l'Environnement, Institut Pierre et Simon Laplace, Commission à l'Énergie Atomique/CNRS/Université de Versailles Saint Quentin en Yveunes–UMR 1572, Avenue de la Terrasse, F-91198 Gif-sur-Yvette Cedex, France. [28]Bruker Nano GmbH, Schwarzschildstraße 12, D-12489 Berlin, Germany. [29]Department of Earth and Environmental Sciences, K.U.Leuven, Box 2408, Celestijnenlaan 200E, 3001 Leuven, Belgium. [30]Natural Resources Canada, Geological Survey of Canada Calgary, 3303 33rd Street NW, Calgary, AB T2L 2A7, Canada. [31]Laboratorio de Paleomagnetismo y Paleoambientes, Programa Universitario de Perforaciones en Oceanos y Continentes, Instituto de Geofísica, Universidad Nacional Autónoma de México (UNAM), DF 04510 Mexico, Mexico. [32]Department of Earth and Ecosystem Sciences, Lund University, Sölvegatan 12, 223 62 Lund, Sweden. [33]Department of Geology and Geophysics, University of Alaska, Fairbanks, AK 99775, USA.

*To whom correspondence should be addressed. E-mail: schulte@geol.uni-erlangen.de. The remaining authors contributed equally to this work.
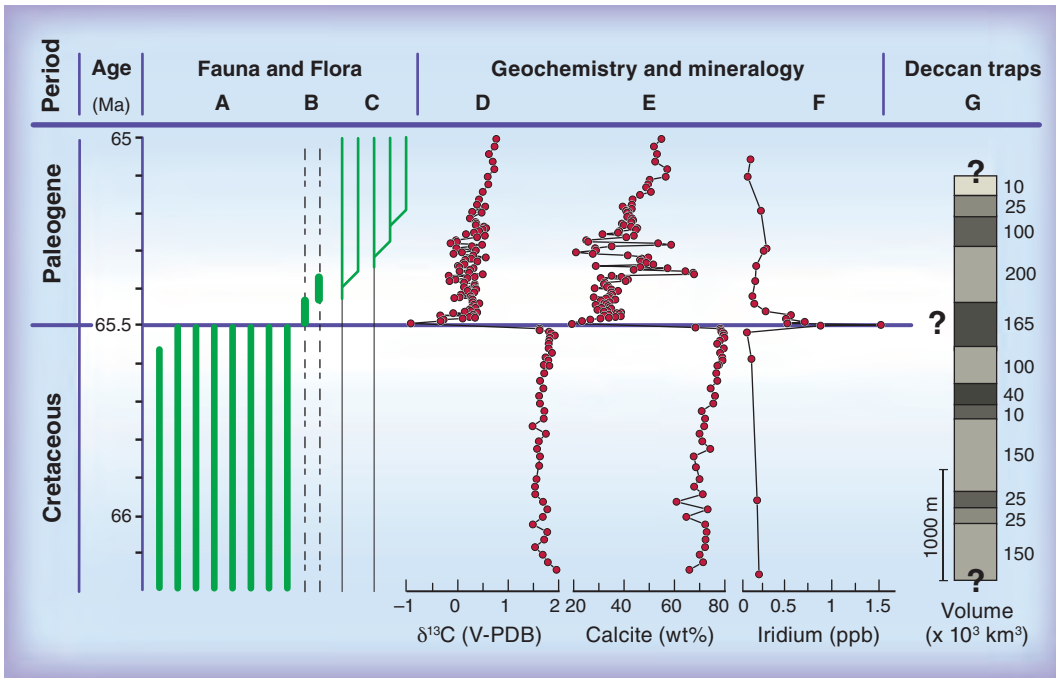
Fig. 1. Stratigraphy and schematic record of biotic events across the K-Pg boundary correlated to the chemical and mineralogical records of a core from the North Atlantic [Ocean Drilling Program (ODP) Leg 207] and the major eruptive units of the Deccan flood basalt province, India. Many (>60%) Cretaceous species experienced mass extinction at the boundary (A), whereas successive blooms of opportunistic species (B) and radiation of new species (C) occurred in the Early Paleogene. V-PDB indicates the Vienna Pee Dee Belemnite; wt %, weight %; and ppb, parts per billion. The mass extinction coincides with a major perturbation of the global carbon cycle as indicated by a negative $\delta^{13}C$ anomaly (D), a major drop of carbonate sedimentation in the marine realm (E), and the enrichment of PGEs in Chicxulub ejecta deposits (F) (25, 26). Composite stratigraphic column of the formations of the main Deccan Trap flood basalt province showing their cumulative thickness and estimated basalt volumes (G) (15). Note that the exact stratigraphic onset and end of the main Deccan flood basalt sequence and the precise position of the K-Pg boundary in the formations have yet to be determined, as indicated by the question marks (16). However, the onset of the main eruption phase is ~400 to 600 thousand years before the K-Pg boundary as is also shown by Os isotope data (38).

K-Pg boundary sites, intercalated between two layers rich in Chicxulub ejecta, suggests that the Chicxulub impact caused a collapse of the Yucatan carbonate platform and triggered mass flows and tsunamis in the Gulf of Mexico and adjacent areas (Fig. 2 and figs. S3 to S8) (17, 18, 30). Therefore, the K-Pg boundary clastic unit, up to 80 m thick in places, was deposited in the extremely brief period between the arrival of coarse-grained spherules and the subsequent, longer-term deposition of the finer-grained PGE- and Ni-rich ejecta phases (Fig. 2) (22).

A contrasting hypothesis is founded on the interpretation that the clastic unit is a long-term depositional sequence genetically unrelated to the Chicxulub impact event (14, 31); lenslike spherule deposits locally present below the clastic unit in Mexico would then correlate to the base of the uppermost Cretaceous planktic foraminiferal zone (14, 31). This interpretation also proposes a latest Cretaceous age for the impact breccia found within the Chicxulub crater with the implication that all intermediate to distal K-Pg boundary sites lack the resolution and completeness to firmly establish a correlation to the Chicxulub impact event (14, 32). Additionally, the assertion that the Chicxulub impact preceded the K-Pg mass extinction by ~300 thousand years predicts that the PGE anomaly at the top of the clastic unit resulted from a second large impact event (14). In this scenario, either the second impact event or the Deccan flood basalt eruptions caused the K-Pg mass extinction (14).

However, sedimentological and petrological data suggest that the lenslike ejecta deposits in Mexico were generated by impact-related liquefaction and slumping, consistent with the single very-high-energy Chicxulub impact (figs. S5 to S9) (23). A range of sedimentary structures and the lack of evidence for ocean floor colonization within the clastic unit in northeastern Mexico indicate rapid deposition (figs. S6 to S8) (22, 23). Moreover, the presence of shallow-water benthic foraminifera in the clastic unit (33) contradicts a long-term depositional sequence (14); if in situ, their presence requires unrealistically rapid relative sea-level changes of >500 m. Lastly, high-resolution planktic foraminiferal analyses in the southern Mexican sections demonstrate that the Chicxulub-linked clastic unit is biostratigraphically equivalent to the officially defined base of the Paleocene (i.e., the red clay

S1) (17, 18). Accordingly, the K-Pg boundary sites can be divided into four groups (Fig. 2 and table S1): (i) In very proximal settings up to 500 km from Chicxulub, impact deposits are quite thick. Cores recovered close to the crater rim inside the Chicxulub impact structure include a >100-m-thick impact-breccia sequence, and 1-m- to >80-m-thick ejecta-rich deposits are present in the surrounding Central American region [e.g., (19–21)]. (ii) In proximal areas around the northwestern Gulf of Mexico from 500 to 1000 km from Chicxulub, the K-Pg boundary is characterized by a series of cm- to m-thick ejecta spherule-rich, clastic event beds indicative of high-energy sediment transport, for example, by tsunamis and gravity flows (18, 22, 23). (iii) At intermediate distances from Chicxulub (~1000 to ~5000 km), the K-Pg boundary deposit consists of a 2- to 10-cm-thick spherule layer topped by a 0.2- to 0.5-cm-thick layer anomalously rich in PGEs with abundant shocked minerals, granitic clasts, and Ni-rich spinels (Fig. 3) (12, 24–26). (iv) In distal marine sections more than 5000 km from Chicxulub, a reddish, 2- to 5-mm-thick clay layer rich in impact ejecta material is usually present at the K-Pg boundary [e.g., (17)]. The

bedding plane between the impact-ejecta-rich red clay layer and the underlying Cretaceous marls coincident with the abrupt mass extinction in the El Kef section, Tunisia, is also the officially defined base of the Paleogene (fig. S1) (27). This definition implies that the impact-generated sediments in the K-Pg boundary interval stratigraphically belong to the Paleogene (Fig. 2).

The pattern of decreasing ejecta-layer thickness with increasing distance from the impact crater is consistent with the Chicxulub impact as the unique source for the ejecta in the K-Pg boundary event deposit (Figs. 2 and 3 and table S1). Additional support for this genetic link derives from the distribution, composition, and depositional mode of the ejecta. First, the size and abundance of spherules and ballistically ejected shocked quartz grains, which are resistant to alteration, decrease with increasing distance from Chicxulub (18, 28). Second, the specific composition [e.g., silicic spherules, shocked limestone, and dolomite and granitic clasts (Fig. 3 and figs. S2 to S4)] (29) and age distribution (table S2) of the ejecta match the suite of Chicxulub target rocks. Lastly, the presence of the high-energy clastic unit at proximal

layer) in the El Kef section, Tunisia (Fig. 2 and fig. S1) (*20*).

A pre–K-Pg boundary age for the Chicxulub event has also been argued on the basis of the sequence at a Brazos River site in Texas and from within the crater. If a 3-cm-thick clay layer interbedded in Upper Cretaceous shales at the Brazos River site originated from the Chicxulub impact, the impact occurred significantly before the K-Pg boundary (*31*). Yet, in this clay layer there are no spherules or shocked minerals that would provide evidence for an impact origin, and its high sanidine and quartz content supports a local volcanic origin similar to ash layers found below the K-Pg boundary in Mexico and Haiti (table S3 and figs. S10 to S12).

Within the Chicxulub crater, an ~50-cm-thick dolomitic sandstone unit between the impact breccias and the lower Paleocene postimpact crater infill has been interpreted as undisturbed sediments deposited immediately after the impact (fig. S13) (*32*). Rare uppermost Cretaceous planktic foraminifera within this unit were proposed as evidence that the impact preceded the K-Pg mass extinction (*32*). However, this sandstone unit is in part cross-bedded, contains ejecta clasts (fig. S14), and also includes planktic foraminifera of Early Cretaceous age (figs. S14 and S15) (*34*, *35*). These observations, as well as grain-size data (*36*), indicate that deposition of this sequence was influenced by erosion and reworking after the impact and therefore provide no evidence for a long-term post-impact and pre–K-Pg boundary deposition.

In addition, multiple independent lines of evidence place the Chicxulub event at the K-Pg boundary. Geochronologic data demonstrate that the Chicxulub impact correlates to the K-Pg boundary at ~65.5 Ma (*29*). Detailed investigation of continuous sequences from globally distributed marine and terrestrial sites yield no chemical or physical evidence of a large impact in the last million years of the Cretaceous other than the Chicxulub event (table S1 and fig. S16) (*25*, *37*, *38*). Lastly, orbital cycles in deep-sea sites [(*39*) and references therein] demonstrate that there is neither a proposed global

300-thousand-year gap (*14*) nor a hiatus between the Chicxulub impact and the K-Pg boundary.

## What Were the Initial Consequences of the Impact?

Asteroid impact models [e.g., (*40*)] predict that an impact large enough to generate the Chicxulub crater would induce earthquakes (magnitude > 11), shelf collapse around the Yucatan platform, and widespread tsunamis sweeping the coastal zones of the surrounding oceans (*7*). Moreover, models

suggest the Chicxulub impact had sufficient energy to eject and distribute material around the globe (*7*), possibly enhanced by decomposition of the volatile-rich carbonate and sulfate sediments (*41*). Near-surface target material was ejected ballistically at velocities up to a few km/s as part of the ejecta curtain. This yielded the thick spherule layer at proximal sites and the basal spherule layer at intermediate distance sites (Fig. 2) (*41*). Parts of the ejecta would be entrained within the impact plume: a complex mixture of hot air;
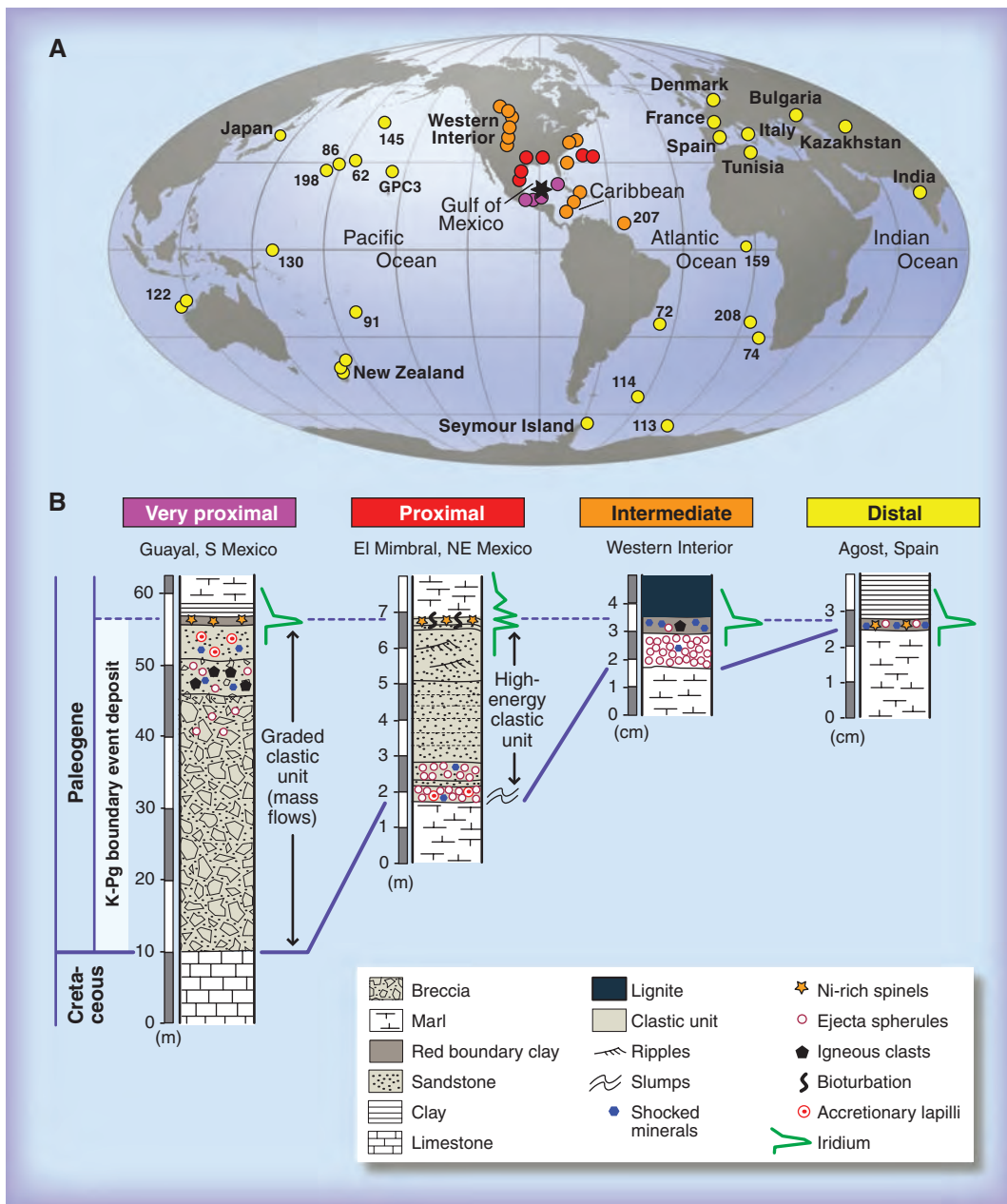
Fig. 2. (**A**) Global distribution of key K-Pg boundary locations. Deep-Sea drill sites are referred to by the corresponding Deep Sea Drilling Project (DSDP) and ODP Leg numbers. The asterisk indicates the location of the Chicxulub impact structure. Colored dots mark the four distinct types of K-Pg boundary event deposit related to distance from the Chicxulub crater (table S1): magenta, very proximal (up to 500 km); red, proximal (up to 1000 km); orange, intermediate distance (1000 to 5000 km); and yellow, distal (>5000 km). Schematic lithologs of the four groups of K-Pg boundary event deposits (**B**) highlighting high-energy event beds (clastic unit) proximal to the crater and the depositional sequence of different materials that originated in one single impact in proximal to distal sites.
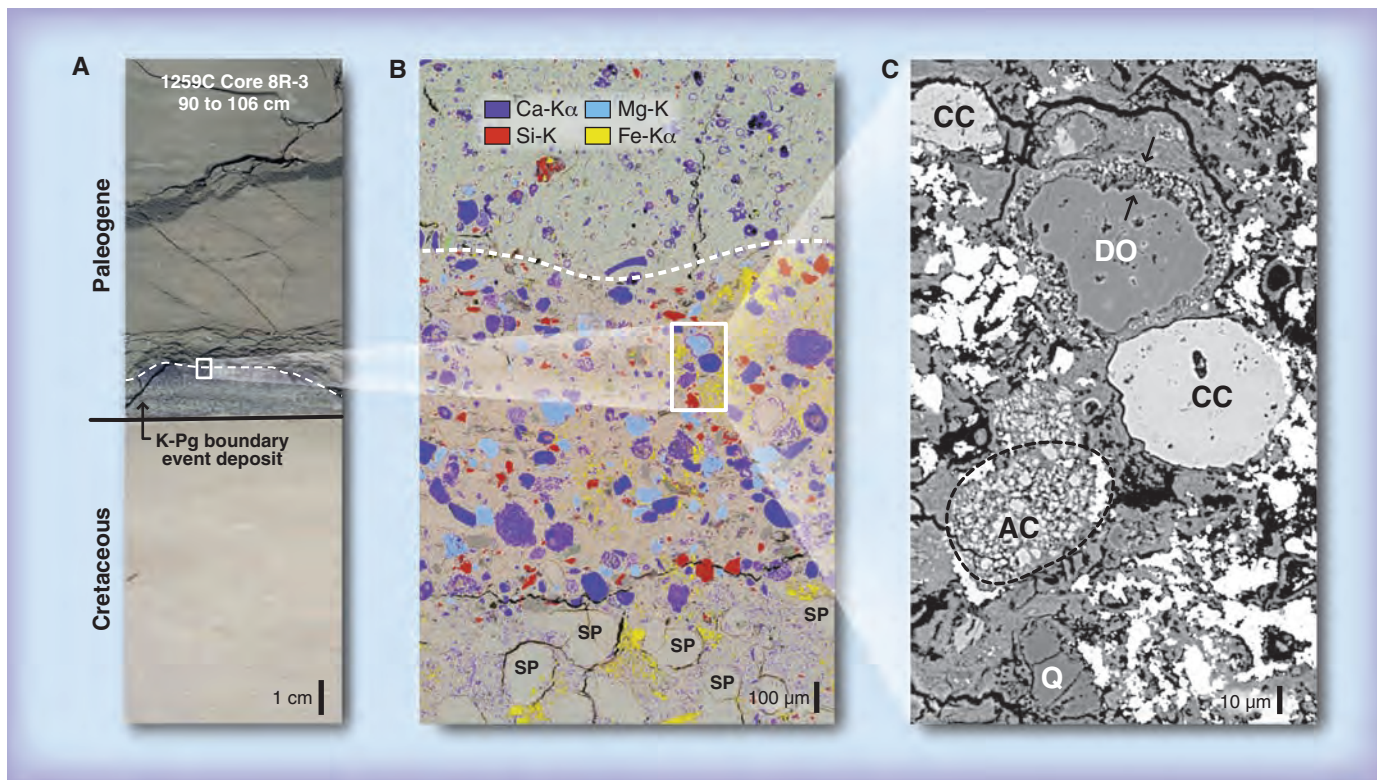
Fig. 3. The K-Pg boundary at ODP Leg 207, western North Atlantic (**A**). An energy-dispersive element distribution map of the box in (A) shows the transition from the top of the spherule-rich graded ejecta sequence (SP) to the lowermost Paleogene sediments (**B**). Note abundant calcite (blue) and dolomite (turquoise) ejecta material as well as occurrence of shocked quartz grains (red) in the uppermost 0.5 mm. A backscattered electron image of the box in (B) shows a rounded dolomite clast (DO) with a Ca-rich clay shell (between arrows), a rounded calcite clast (CC), an accretionary calcite clast (AC), and quartz (Q) interpreted to be of shock-metamorphic origin resulting from the Chicxulub impact (**C**).

projectile material; and impact-vaporized, shock-melted, and fragmented target rocks that expanded rapidly by several km/s up to velocities greater than Earth's escape velocity of 11 km/s. Projectile-rich impact plume deposits form the upper layer in intermediate-distance K-Pg sections and contribute to the single red K-Pg boundary clay layer at distal sites, enriching both in PGEs and shocked minerals (Fig. 2).

Detailed multiphase flow models suggest that the atmospheric reentry of the ejecta spherules may have caused a global pulse of increased thermal radiation at the ground (42). Such a thermal pulse is below the lower limits of woody biomass ignition, in agreement with studies yielding no evidence for widespread large wildfires at the K-Pg boundary (43), with a possible exception for the Gulf of Mexico region close to the impact site [(9) and references therein]. However, the modeled level of radiation is expected to have resulted in thermal damage to the biosphere even if the maximum radiation intensity was only sustained for a few minutes.

Geophysical models indicate that the impact release of large quantities of water, dust, and climate-forcing gases would dramatically alter the climate system (7, 8). The estimated amount of the silicic sub-micrometer-sized dust input of 0.01 to 0.1 Gt ($1 \text{ Gt} = 10^{15}$ g) is considered to be too low by itself to cause a catastrophic impact winter (44).

However, abundant sub-micrometer-sized particulate carbonates in the ejecta (26) and soot, a strong absorber of short-wave radiation, derived from burning of targeted carbonaceous sediments may have greatly amplified the effects of dust injection (43). In addition, there are estimates of at least 100 to 500 Gt of sulfur released nearly instantaneously (7, 8). These figures are likely to be conservative given new larger estimates of the volume of water and sulfur-bearing sediments within Chicxulub's 100-km-diameter transient crater (45). The sulfur was probably rapidly transformed to sunlight-absorbing sulfur aerosols with the capacity to cool Earth's surface for years to decades by up to 10°C (8, 10). Temperatures of the deep ocean, however, remained largely unaffected by the impact because of the ocean's large thermal mass (46), contributing to a rapid recovery of the global climate. The sulfur release also generated acid rain, which, although not sufficient to completely acidify ocean basins, would have severely affected marine surface waters and/or poorly buffered continental catchments and watersheds (9).

Although current models cannot fully assess the combined environmental consequences of the Chicxulub impact (7, 9), the extremely rapid injection rate of dust and climate-forcing gases would have magnified the environmental consequences compared with more-prolonged volcanic eruptions, particularly when compounded by the additional adverse effects of a large impact (e.g., heat wave, soot, and dust release) that are absent during flood basalt volcanism. Specifically, the injection of ~100 to 500 Gt of sulfur into the atmosphere within minutes after the Chicxulub impact contrasts with volcanic injection rates of 0.05 to 0.5 Gt of sulfur per year during the ~1-million-year-long main phase of Deccan flood basalt volcanism (Fig. 1 and fig. S16) (15, 16). Indeed, an only moderate climate change (~2°C warming) during the last 400 thousand years of the Cretaceous has been interpreted to result from Deccan flood basalt volcanism [e.g., (47)].

What Does the Fossil Record Reveal About the Global Consequences for Life?

The scale of biological turnover between the Cretaceous and Paleogene is nearly unprecedented in Earth history (1). A number of major animal groups disappeared across the boundary (e.g., the nonavian dinosaurs, marine and flying reptiles, ammonites, and rudists) (48), and several other major groups suffered considerable, but not complete, species-level extinction (e.g., planktic foraminifera, calcareous nannofossils, land plants) (12, 13, 37, 49). Even the groups that showed negligible extinctions exhibited substantial changes in assemblage composition (e.g., benthic foraminifera) (50).

For marine phytoplankton, major drivers of ocean productivity, darkness, and suppression of photosynthesis were likely major killing

mechanisms (9). There is a clear separation in extinction rate between strongly affected phytoplankton groups with calcareous shells and groups that had organic or siliceous shells. Although the possible effects of surface ocean acidification after the impact may have been an additional stress factor, this selectivity seems to have favored traits contributing to survival of acute stress (11, 13). For example, cyst-forming dinoflagellates persisted through the K-Pg boundary, although assemblage changes suggest a brief cooling phase after the impact [(51) and references therein].

The extinction of calcareous primary producers must have caused major starvation higher up in the food chain. This would explain the extinctions of animals relying on plankton as their food source, the survival of organisms living in detritus-based food chains, and the dwarfing in evolutionary lineages observed in marine biota after the K-Pg boundary (9, 52, 53). The abrupt drop in plankton productivity was apparently short-lived as shown by marine biomarker data (54). The negative shift of the stable carbon isotopic value (δ^{13}C) (Fig. 1) and the surface to deep water δ^{13}C gradient collapse is indicative of a major disruption to marine productivity and the ocean's biological pump (11). However, the large magnitude of the δ^{13}C anomaly suggests that the release of methane, input of soot, or the dependency of the isotopic signal on the metabolism of different species may have contributed to the anomaly (50).

On land, the loss of the diverse vegetation and the onset of the fern-spore spike following the K-Pg boundary indicates instantaneous (days to months) destruction of diverse forest communities coincident with deposition of ejecta from the Chicxulub impact (fig. S17) (12, 37, 55). A shutdown of photosynthesis because of low light levels is also indicated by high abundances of fungal spores in a thin layer of sediment preceding the recovery succession of ferns at a New Zealand K-Pg boundary site (56). Analogous to the marine environment, the abrupt elimination of the forest communities may have had similarly catastrophic effects on animals relying on primary producers (e.g., the herbivorous dinosaurs), whereas detritus-based food chains (e.g., in lakes) were apparently less affected (52).

Faunal and floral changes during the Late Cretaceous do occur [e.g., (12, 47)] but are clearly distinguishable from the abrupt mass extinction and ecosystem disruption coincident with the K-Pg boundary, as indicated by high-resolution records of marine planktonic microfossils and terrestrial pollen and spores (12, 13, 25, 37, 55, 57). Productivity proxies (e.g., carbonate content) linked to orbitally tuned stratigraphic time scales provide no evidence for major changes preceding the boundary (39). Claims of gradual or stepwise extinctions during the Late Cretaceous culminating in the K-Pg mass extinction (14) and survivorship through the K-Pg boundary may be explained by short-term survival with greatly reduced population sizes, sampling artifacts, or reworking of Cretaceous fossils [e.g., (57)]. In addition, the global onset of opportunistic species blooms and the evolutionary radiation of new taxa started consistently after the K-Pg boundary mass extinction (Fig. 1 and fig. S17) (49, 55).

What Do We Need to Look at Next?

The correlation between impact-derived ejecta and paleontologically defined extinctions at multiple locations around the globe leads us to conclude that the Chicxulub impact triggered the mass extinction that marks the boundary between the Mesozoic and Cenozoic eras ~65.5 million years ago. This conclusion is reinforced by the agreement of ecological extinction patterns with modeled environmental perturbations. Although the relative importance of the different impact-induced environmental effects on the K-Pg mass extinction is still under scrutiny, alternative multi-impact or volcanic hypotheses fail to explain the geographic and stratigraphic distribution of ejecta and its composition, the timing of the mass extinction, and the scale of environmental changes required to cause it. Future geophysical, geological, and drilling studies of the Chicxulub structure will further constrain the impact process and the amount and nature of environment-altering gases generated by this so far unparalleled combination of a large impact into ~3- to 4-km-thick carbonate- and sulfate-rich target rocks. Research focused on high-resolution studies of the ejected material, integrated climate models, and detailed study of related fossil successions will help reveal the physical and biological mechanisms of the K-Pg mass extinction and may also aid in understanding other mass extinction events in Earth history.

References and Notes

1. J. Alroy, *Proc. Natl. Acad. Sci. U.S.A.* **105** (suppl. 1), 11536 (2008).
2. L. W. Alvarez, W. Alvarez, F. Asaro, H. V. Michel, *Science* **208**, 1095 (1980).
3. J. Smit, J. Hertogen, *Nature* **285**, 198 (1980).
4. A. Montanari et al., *Geology* **11**, 668 (1983).
5. B. F. Bohor, *Tectonophysics* **171**, 359 (1990).
6. A. R. Hildebrand et al., *Geology* **19**, 867 (1991).
7. O. B. Toon, K. Zahnle, D. Morrison, R. P. Turco, C. Covey, *Rev. Geophys.* **35**, 41 (1997).
8. E. Pierazzo, A. N. Hahmann, L. C. Sloan, *Astrobiology* **3**, 99 (2003).
9. D. A. Kring, *Palaeogeogr. Palaeoclimatol. Palaeoecol.* **255**, 4 (2007).
10. K. O. Pope, K. H. Baines, A. C. Ocampo, B. A. Ivanov, *J. Geophys. Res.* **102**, (E9), 21645 (1997).
11. S. D'Hondt, *Annu. Rev. Ecol. Evol. Syst.* **36**, 295 (2005).
12. A. R. Sweet, D. R. Braman, *Can. J. Earth Sci.* **38**, 249 (2001).
13. P. Bown, *Geology* **33**, 653 (2005).
14. G. Keller, W. Stinnesbeck, T. Adatte, D. Stüben, *Earth Sci. Rev.* **62**, 327 (2003).
15. S. Self, M. Widdowson, T. Thordarson, A. E. Jay, *Earth Planet. Sci. Lett.* **248**, 518 (2006).
16. A.-L. Chenet et al., *J. Geophys. Res.* **114**, (B6), B06103 (2009).
17. J. Smit, *Annu. Rev. Earth Planet. Sci.* **27**, 75 (1999).
18. P. Claeys, W. Kiessling, W. Alvarez, *Spec. Pap. Geol. Soc. Am.* **356**, 55 (2002).
19. J. Urrutia-Fucugauchi, L. E. Marín, A. Trejo-Garcia, *Geophys. Res. Lett.* **23**, 1565 (1996).
20. I. Arenillas et al., *Earth Planet. Sci. Lett.* **249**, 241 (2006).
21. K. Goto et al., *Cretaceous Res.* **29**, 217 (2008).
22. J. Smit, W. Alvarez, A. Montanari, P. Claeys, J. M. Grajales-Nishimura, *Spec. Pap. Geol. Soc. Am.* **307**, 151 (1996).
23. P. Schulte, A. Kontny, *Spec. Pap. Geol. Soc. Am.* **384**, 191 (2005).
24. R. D. Norris, B. T. Huber, B. T. Self-Trail, *Geology* **27**, 419 (1999).
25. K. G. MacLeod, D. L. Whitney, B. T. Huber, C. Koeberl, *Geol. Soc. Am. Bull.* **119**, 101 (2007).
26. P. Schulte et al., *Geochim. Cosmochim. Acta* **73**, 1180 (2009).
27. E. Molina et al., *Episodes* **29**, 263 (2006).
28. J. V. Morgan et al., *Earth Planet. Sci. Lett.* **251**, 264 (2006).
29. Materials and methods are available as supporting material on *Science* Online.
30. T. J. Bralower, C. K. Paull, R. M. Leckie, *Geology* **26**, 331 (1998).
31. G. Keller et al., *Earth Planet. Sci. Lett.* **255**, 339 (2007).
32. G. Keller et al., *Meteorit. Planet. Sci.* **39**, 1127 (2004).
33. L. Alegret, E. Molina, E. Thomas, *Geology* **29**, 891 (2001).
34. J. A. Arz, L. Alegret, I. Arenillas, *Meteorit. Planet. Sci.* **39**, 1099 (2004).
35. J. Smit, S. V. D. Gaast, W. Lustenhouwer, *Meteorit. Planet. Sci.* **39**, 1113 (2004).
36. T. J. Bralower et al., *Geology*, in press.
37. D. J. Nichols, K. R. Johnson, *Plants and the K-T Boundary* (Cambridge Univ. Press, Cambridge, 2008), p. 280.
38. N. Robinson, G. Ravizza, R. Coccioni, B. Peucker-Ehrenbrink, R. D. Norris, *Earth Planet. Sci. Lett.* **281**, 159 (2009).
39. T. Westerhold et al., *Palaeogeogr. Palaeoclimatol. Palaeoecol.* **257**, 377 (2008).
40. B. Ivanov, *Sol. Syst. Res.* **39**, 381 (2005).
41. N. Artemieva, J. Morgan, *Icarus* **201**, 768 (2009).
42. T. J. Goldin, H. J. Melosh, *Geology* **37**, 1135 (2009).
43. M. C. Harvey, S. C. Brassell, C. M. Belcher, A. Montanari, *Geology* **36**, 355 (2008).
44. K. O. Pope, *Geology* **30**, 99 (2002).
45. S. P. S. Gulick et al., *Nat. Geosci.* **1**, 131 (2008).
46. T. Luder, W. Benz, T. F. Stocker, *J. Geophys. Res.* **108**, (E7), 5074 (2003).
47. P. Wilf, K. R. Johnson, B. T. Huber, *Proc. Natl. Acad. Sci. U.S.A.* **100**, 599 (2003).
48. D. E. Fastovsky, P. M. Sheehan, *GSA Today* **15**, 4 (2005).
49. I. Arenillas, J. A. Arz, E. Molina, C. Dupuis, *Micropaleontology* **46**, 31 (2000).
50. E. Thomas, *Spec. Pap. Geol. Soc. Am.* **424**, 1 (2007).
51. P. S. Willumsen, *Cretaceous Res.* **27**, 954 (2006).
52. P. M. Sheehan, P. J. Coorough, D. E. Fastovsky, *Spec. Pap. Geol. Soc. Am.* **307**, 477 (1996).
53. M. Aberhan, S. Weidemeyer, W. Kiessling, R. A. Scasso, F. A. Medina, *Geology* **35**, 227 (2007).
54. J. Sepúlveda, J. E. Wendler, R. E. Summons, K.-U. Hinrichs, *Science* **326**, 129 (2009).
55. V. Vajda, J. I. Raine, C. J. Hollis, *Science* **294**, 1700 (2001).
56. V. Vajda, S. McLoughlin, *Science* **303**, 1489 (2004).
57. C. R. C. Paul, *Palaeogeogr. Palaeoclimatol. Palaeoecol.* **224**, 291 (2005).
58. D.J.N. passed away during the final revision of this paper. His more than 30 years of work on the Cretaceous-Paleogene boundary influenced the data, ideas, and thesis of this paper. This research used samples and photos provided by the Ocean Drilling Program (ODP) and the International Continental Scientific Drilling Program (ICDP) and was funded by the Deutsche Forschungsgemeinschaft, the Austrian Science Foundation (FWF), Danish Carlsberg Foundation, European Social Fund, Research Foundation Flanders, Mexican Consejo Nacional de Ciencia y Tecnología, NASA, Japan Society for the Promotion of Science, Joint Oceanographic Institutions, K.U.Leuven Research Fund, UK Natural Environment Research Council, NSF, the Swedish Research Council (VR) and the Royal Swedish Academy of Sciences through the Knut and Alice Wallenberg Foundation, and the Spanish Ministerio de Ciencia e Innovación. We are grateful to E. Thomas and an anonymous reviewer for valuable comments and thank G. Izett for providing support and photos.

Supporting Online Material for

The Chicxulub Asteroid Impact and Mass Extinction at the Cretaceous-Paleogene Boundary

Peter Schulte,* Laia Alegret, Ignacio Arenillas, Jose A. Arz, Penny J. Barton, Paul R. Bown, Timothy J. Bralower, Gail L. Christeson, Philippe Claeys, Charles S. Cockell, Gareth S. Collins, Alexander Deutsch, Tamara J. Goldin, Kazuhisa Goto, José M. Grajales-Nishimura, Richard A. F. Grieve, Sean P. S. Gulick, Kirk R. Johnson, Wolfgang Kiessling, Christian Koeberl, David A. Kring, Kenneth G. MacLeod, Takafumi Matsui, Jay Melosh, Alessandro Montanari, Joanna V. Morgan, Clive R. Neal, Douglas J. Nichols, Richard D. Norris, Elisabetta Pierazzo, Greg Ravizza, Mario Rebolledo-Vieyra, Wolf Uwe Reimold, Eric Robin, Tobias Salge, Robert P. Speijer, Arthur R. Sweet, Jaime Urrutia-Fucugauchi, Vivi Vajda, Michael T. Whalen, Pi S. Willumsen

*To whom correspondence should be addressed. E-mail: schulte@geol.uni-erlangen.de

This PDF file includes:

Materials and Methods
SOM Text
Figs. S1 to S17
Tables S1 to S3
References

Materials and Methods

1. Mineralogy – The mineral composition of samples from the Ocean Drilling Project (ODP) Leg 207 Site 1259C and the Brazos River Cretaceous-Paleogene (K-Pg) sections was determined at the University of Erlangen on wet powdered samples (grain size <10 µm obtained with a McCrone Micromill) (*S1*) with a Siemens D5000 X-ray diffractometer. Powdered samples were scanned from 5° to 85° 2Θ with steps of 0.2° and a scanning time of 4 seconds. Spectra were evaluated by the quantitative Rietveld analysis with the BGMN Version 4.1.1 software (www.bgmn.de). The analytical error is <3% relative. Within BGMN, we used corrections for tube tails, sample zero point and sample eccentricity. The background was reduced to a 5-fold polynome to accommodate disordered phases. In addition, only the range between 10 and 65° 2Θ was fitted with BGMN to avoid problems in the high-angle range. The total number of parameters was 102-148, depending on automatic reducing the order of preferred orientation correction in cases of low phase content.

2. Stable isotopes – Samples from the K-Pg transition in the ODP Leg 207 Site 1259C were disintegrated in deionized water using a small amount of H_2O_2 then washed over a 63 µm sieve. Subsequently, the fine fraction (<63 µm) was separated and powdered. The fine fraction powder reacted with 100% phosphoric acid at 75°C using a Kiel III online carbonate preparation line connected to a ThermoFinnigan 252 mass spectrometer at the University of Erlangen (Germany). All values are reported in ‰ relative to VPDB by assigning a $\delta^{13}C$ value of +1.95 ‰ and a $\delta^{18}O$ value of –2.20 ‰ to NBS19. Reproducibility was determined by replicate analysis of laboratory standards and is better than ±0.05 and 0.06 ‰ (1σ) for $\delta^{13}C$ and $\delta^{18}O$, respectively.

3. Electron microprobe: Wavelength-dispersive (WDS) and energy-dispersive (EDS) electron microprobe (EMP) analyses, as well as back-scattered electron (BSE) images of ejecta components were performed with the JEOL JXA-8200 Superprobe (GeoZentrum Nordbayern, Universität Erlangen), equipped with four WDS spectrometers, an EDS system and an electron backscatter detector. In addition, at BRUKER AXS Microanalysis GmbH, Berlin, fast high-resolution element scans were conducted with a JEOL JSM-6490LV electron microscope equipped with a Quantax EDS system including a liquid nitrogen free XFlash 4010 and 4030 EDS silicon drift detector (SDD) and the Esprit 1.8 software using 15 kV acceleration voltage, counting rates between 100 and 220 kcps, and integration times of 10–20 min for a mapping resolution of 1600 x1200 pixel.

Supporting Text, Tables and Figures

Definition of the Cretaceous-Paleocene boundary

The base of the Danian Stage, i.e. Cretaceous-Paleogene (K-Pg; formerly K-T) boundary was formally delineated by the International Commission on Stratigraphy (ICS) at the base of the dark clay bed commonly called the "K-Pg boundary clay" in the Cretaceous-Paleogene Global Boundary Stratotype Section and Point (GSSP) at El Kef, Tunisia (*S2*). It is an undisturbed and continuos K-Pg boundary section and shows the coincidence of the mass extinction of marine plankton (calcareous nannofossils and planktonic foraminifera), ecological disruption at the sea floor (benthic foraminifera), drop in carbonate content, and perturbation of the global carbon cycle at the impact level [Fig. S1, (*S2*)]. This impact level, which we correlate to the Chicxulub impact, is present at base of the boundary clay and is characterized by a millimeter thick red clay layer that includes an Ir anomaly, ejecta spherules, and Ni-rich spinel (*S2*). There is no evidence for major extinctions or trends indicating ecological stress such as temperature change foreshadowing the K-Pg event in this section (*S3-S5*). Meanwhile, several auxiliary K-Pg boundary sections have been proposed and correlated to the El Kef section, including the Aïn Settera and Ellès sections (Tunisia), the Caravaca and Zumaya sections (Spain), the Bidart section (France), and the El Mulato and Bochil sections (Mexico) (*S6*).

Chicxulub impact ejecta at the K-Pg boundary

The petrography, composition, and age of ejecta material present in K-Pg boundary sites match the suite of target rocks within the Chicxulub crater. These target rocks include granitic to gneissic basement of Pan-African or older age, and Jurassic-Cretaceous carbonates, black shales, and evaporites (e.g., *S7-S9*).

(i) Shocked zircons from the ejecta deposits in Beloc, Haiti, and the K-Pg boundary event deposit in several sites in North America yield common U-Pb ages of 545±5 million years ago (Ma), in agreement with the Pan-African basement ages reported from crystalline clasts in breccias from the Chicxulub crater (Table S2) (*S10*).

(ii) Relict glass particles and vesicular ejecta spherules with a composition similar to Chicxulub melt rocks and unshocked feldspar and gneiss fragments that match the granitic to gneissic basement of Chicxulub are present in the event deposit at several intermediate distance and distal K-Pg boundary sites (Fig. S3) (*S11-S16*).

(iii) Accretionary calcite and dolomite clasts showing evidence of strong thermal metamorphism and fragments of shallow water limestone and dolomite are present in the event deposit at several proximal to intermediate distance K-Pg boundary sites, e.g., from all K-Pg sites in northeastern Mexico, from Brazos, Texas (*S17*), Ocean Drilling Program (ODP) Site 171, northwestern Atlantic (*S12*), ODP Leg 174AX, northwestern Atlantic (*S17*), ODP Site 207, tropical western North Atlantic (Fig. 3 and Figs. S3 to S5) (*S16*). The presence of textures indicative of shock-metamorphism and thermal alteration in these carbonate clasts suggest that they were ejected by the Chicxulub impact.

(iv) High concentrations of carbon cenospheres and soot in the red K-Pg boundary clay from several sites in North America, Denmark, and New Zealand are interpreted to derive from incomplete combustion of coal or petroleum droplets, probably from Jurassic-Cretaceous black shales in the Yucatán carbonate platform close to Chicxulub (*S18*, *S19*).

(v) Kuiper et al. (*S20*) used a combination of orbital chronology and geochronology to arrive at a new estimate for the absolute age of the K-Pg boundary of ~65.95 million years ago. These authors provided also an assessment of geochronologic data constraining the ages of the Chicxulub impact crater and spherules from proximal to intermediate K-Pg boundary sections (see Table 1 in *S20*). Kuiper et al. (*S20*) concluded that there is no indication that the age of the Chicxulub impact melt lithologies predate the K-Pg boundary by 300 thousand years and indicated that rather the available ages of Chicxulub melt rocks and the shocked minerals and ejecta spherules from the K-Pg boundary in Northern America are indistinguishable within an uncertainty of <100 thousand years.

(vi) Alvarez et al. (*S21*) report a one million year-long iridium record from Gubbio, Italy, demonstrating that this well documented pelagic sequence contains no evidence of multiple Ir anomalies. This result was recently confirmed by additional high resolution iridium data from a nearby section and two additional ocean drilling sites complemented by associated Os isotope data (*S22*) (see also Fig. S16 for a partial reproduction of the Os isotope data).
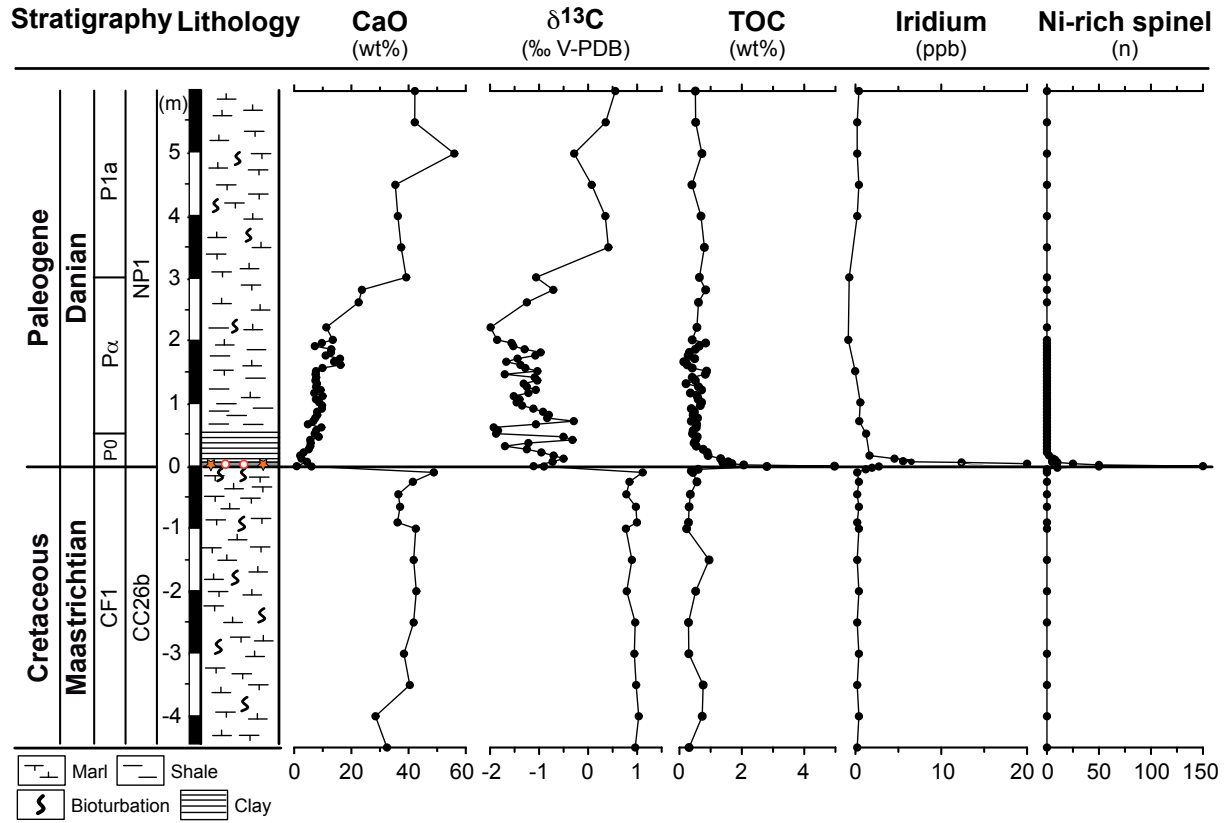
Figure S1. Integrated stratigraphy and geochemistry across the K-Pg boundary in the El Kef GSSP section (δ^{13}C data derived from bulk rock analysis; data compiled from *S2*, *S5*, *S23*, S*24*).
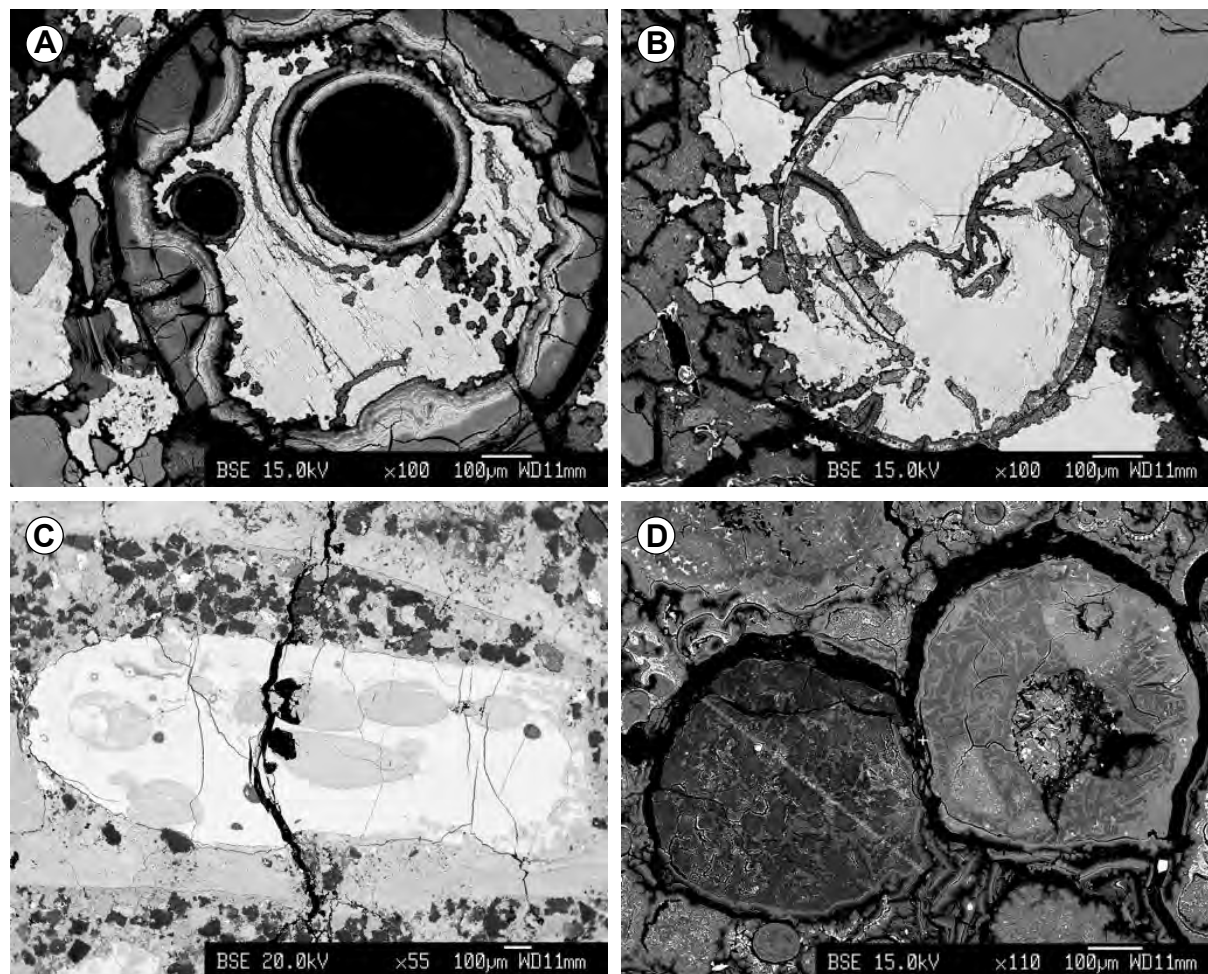
Figure S2: Backscattered-electron (BSE) images of typical ejecta spherules from the K-Pg event deposit. (**A**) and (**B**) Rounded and vesicular spherules from the Shell Creek site, Alabama (see *S25* for locality and lithology) that consist of a smectite shell and a calcite infilling. Note welding of two spherules in (B). (**C**) A dumbell-shaped spherule from the La Popa Basin, Mexico (sample from the base of section E4 in *S26*). The bright gray appearance of the spherule results from the high Fe- and Mg-contents that is a typical feature of the spherules in northeastern Mexico (*S27*). (**C**) Two smectite spherules from the ODP Leg 207, Demerara Rise, western tropical North Atlantic. Difference in grey tones result from different smectite compositions with the spherule to the right showing significant higher Fe- and Mg-contents than the spherule to the left. Note also presence of smectite pseudomorphs after lath-shaped crystals which represent a primary feature that reflects rapid cooling from a melt (*S16*).
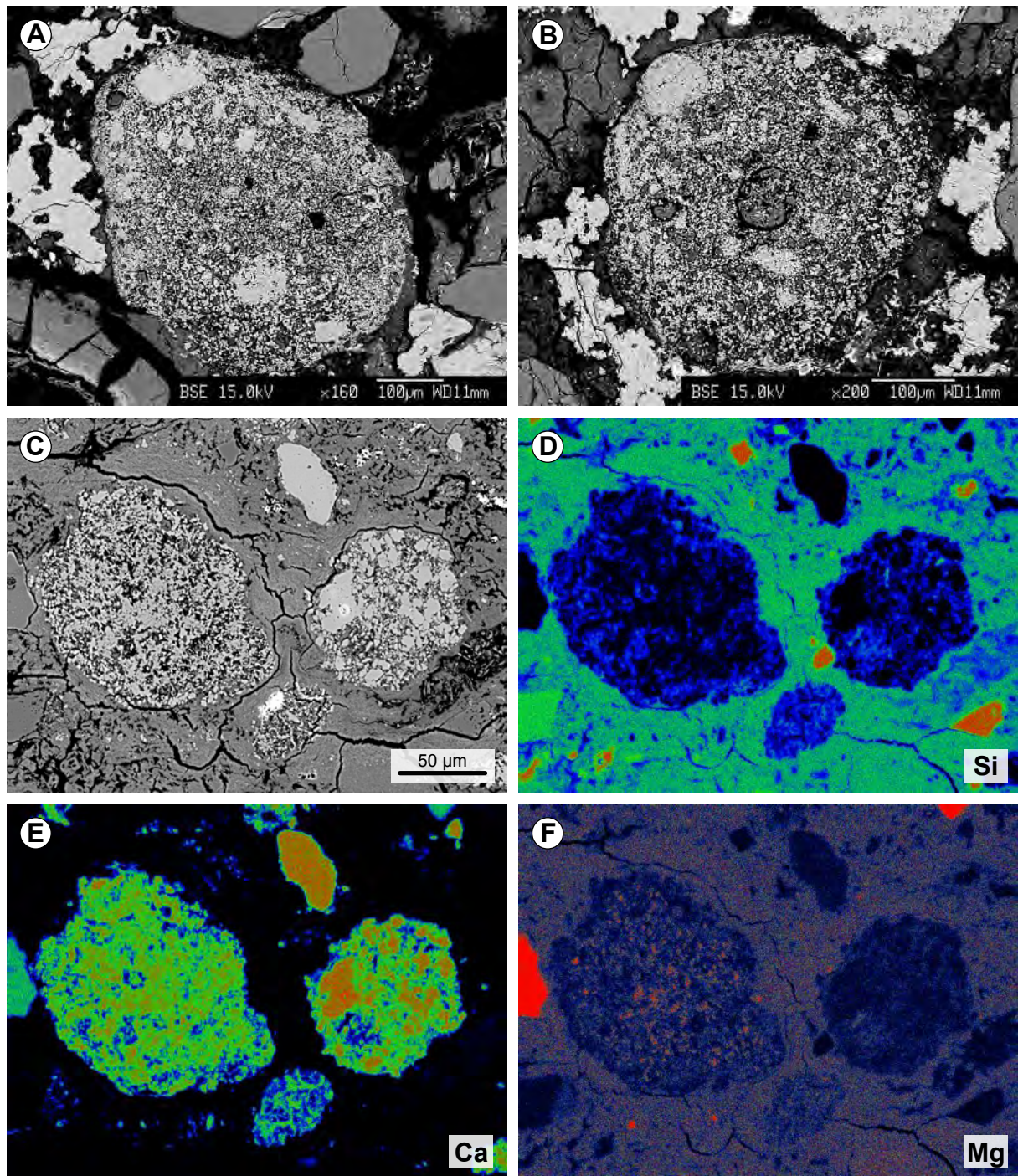
Figure S3: Accretionary carbonate clasts from the K-Pg event deposit. (**A**) and (**B**) BSE images of typical carbonate clasts from the Shell Creek site, Alabama which are similar to the carbonate clasts described from the Brazos site, Texas (*S17*). (**C**) to (**F**) BSE image and energy-dispersive (EDS) elemental maps from two accretionary carbonate clasts from the topmost 0.5 mm of the event deposit in ODP Leg 207, Demerara Rise, West Atlantic (see also Fig. 3). Note slight enrichment of Mg in the left clast. Spectrum from black to blue, green, and red corresponds to increasing element abundance.
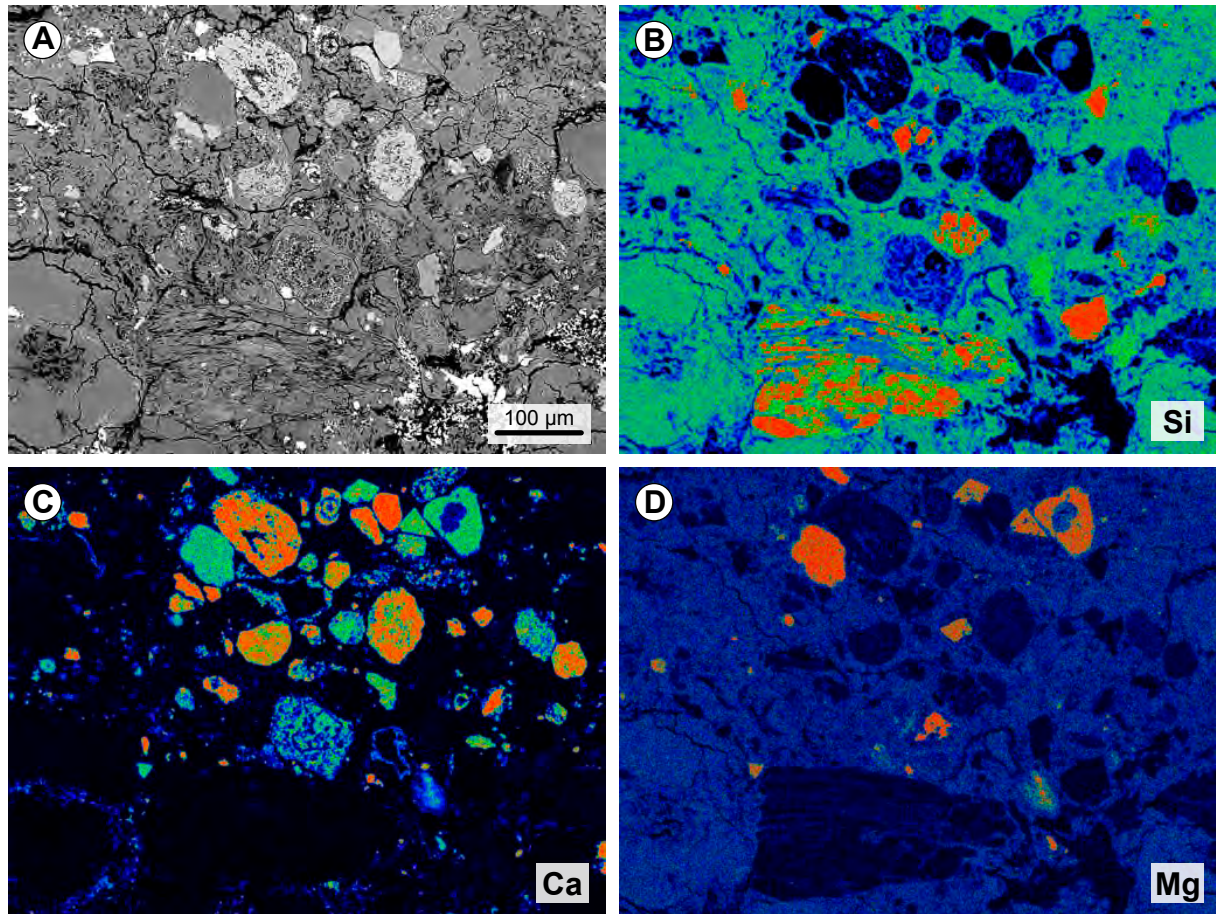
Figure S4: BSE image and EDS elemental maps showing the topmost 0.5 mm of the event deposit in ODP Leg 207, Demerara Rise, tropical western North Atlantic. Note complex composition of the event bed with various types of accretionary carbonate clasts, dolomite clasts, large lithic, quartz grains, and a large lithic clast in the lower part consisting of feldspar, mica, and quartz. This grain is 200 x 350 μm in size and probably a gneiss clast (*S16*). For additional details see Fig. 3.
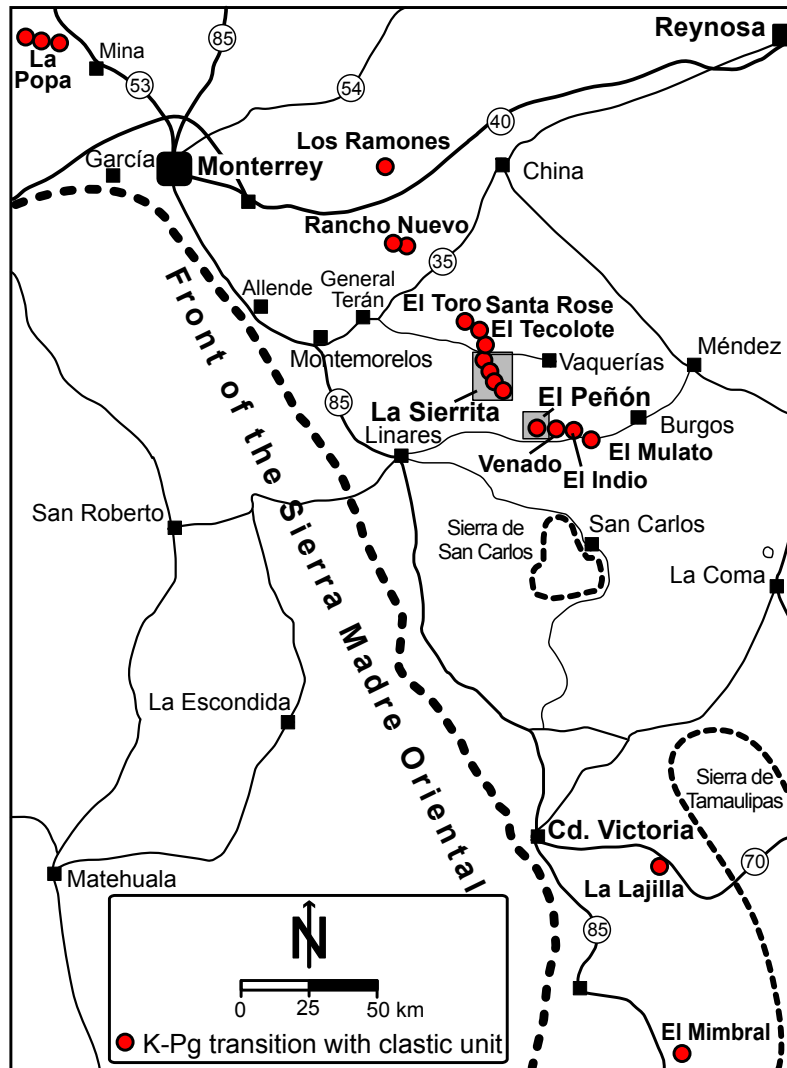
Figure S5: Overview map of the K-Pg boundary sections in NE Mexico. Note that slumped, lens-like ejecta deposits within upper Maastrichtian marls have only been reported from two outcrops (La Sierrita and El Peñón) (*S28, S29*).
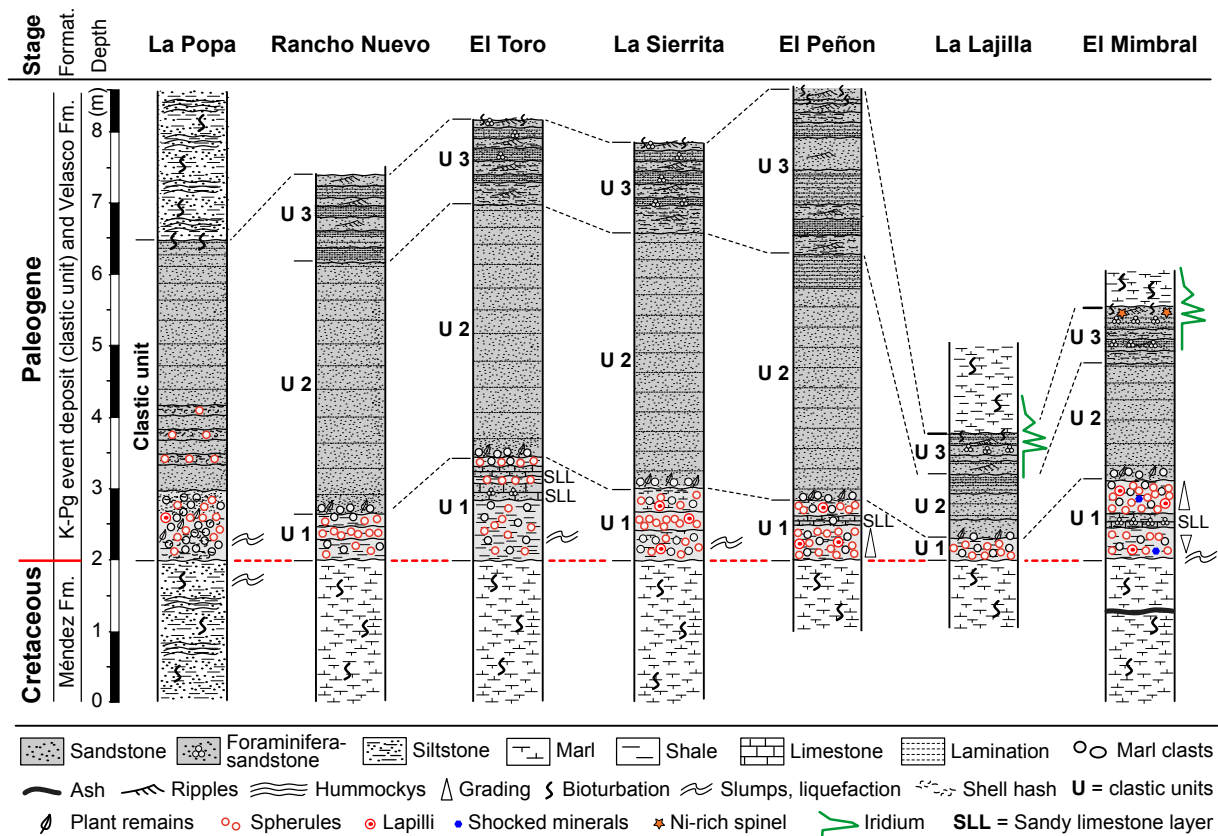
Figure S6: Schematic lithological columns of the clastic unit in NE Mexico. This transect spans the northernmost K-Pg boundary sections outcrops in the La Popa Basin up to the El Mimbral outcrop. Note similarity of the depositional sequence across a distance of 300 km (compiled from *S26*, *S27,* and *S30*). The sedimentary sequence in the La Popa basin is distinct as this is a inner neritic setting, compared to the bathyal settings of all other K-Pg sites in NE Mexico. Ir abundance schematically drawn after Smit et al. (*S30*) for the El Mimbral sections, and after Lindenmaier et al. (*S31*) for the La Lajilla sections. Ni-rich spinel data are from Rocchia et al. (*S24*).
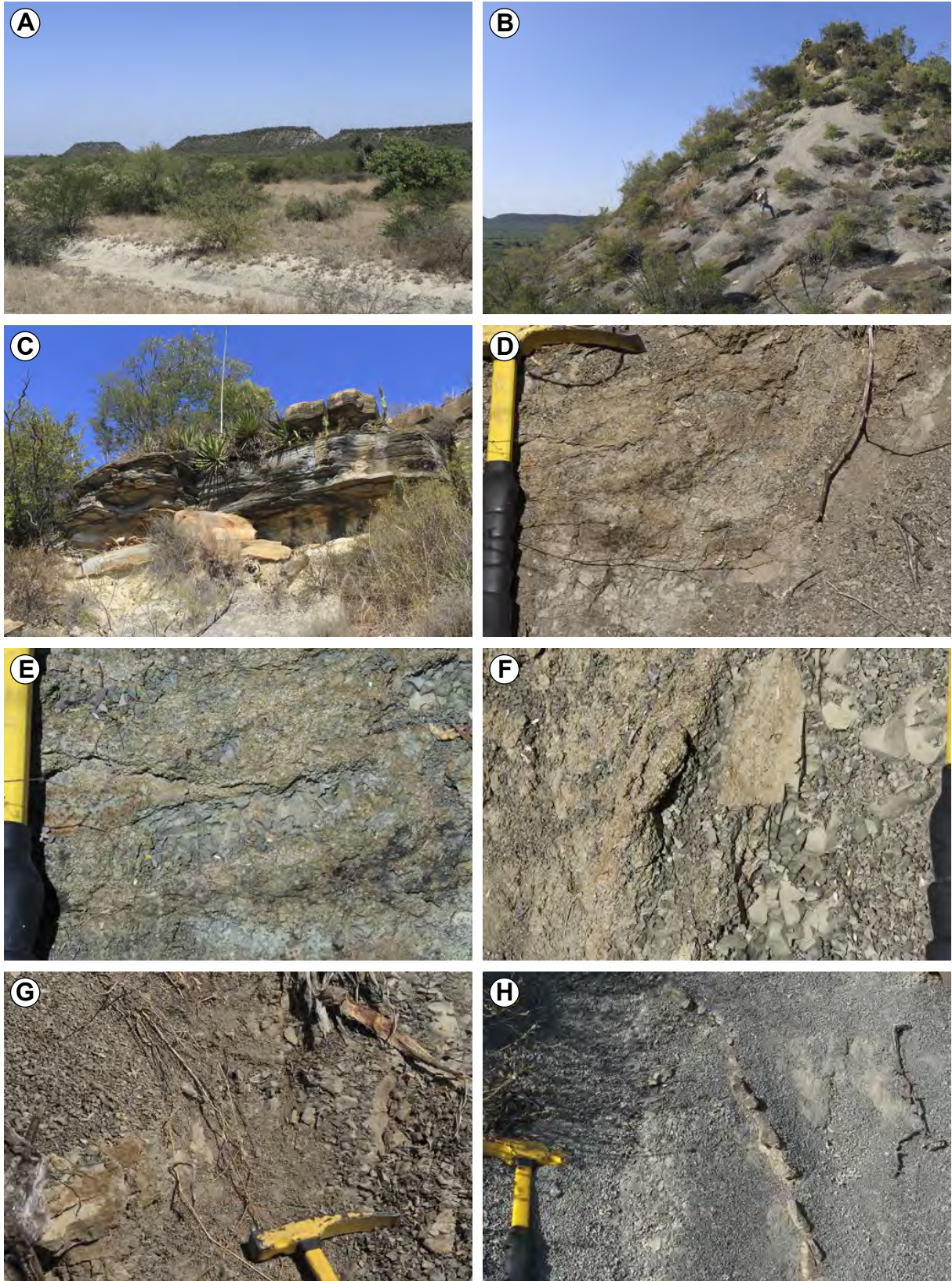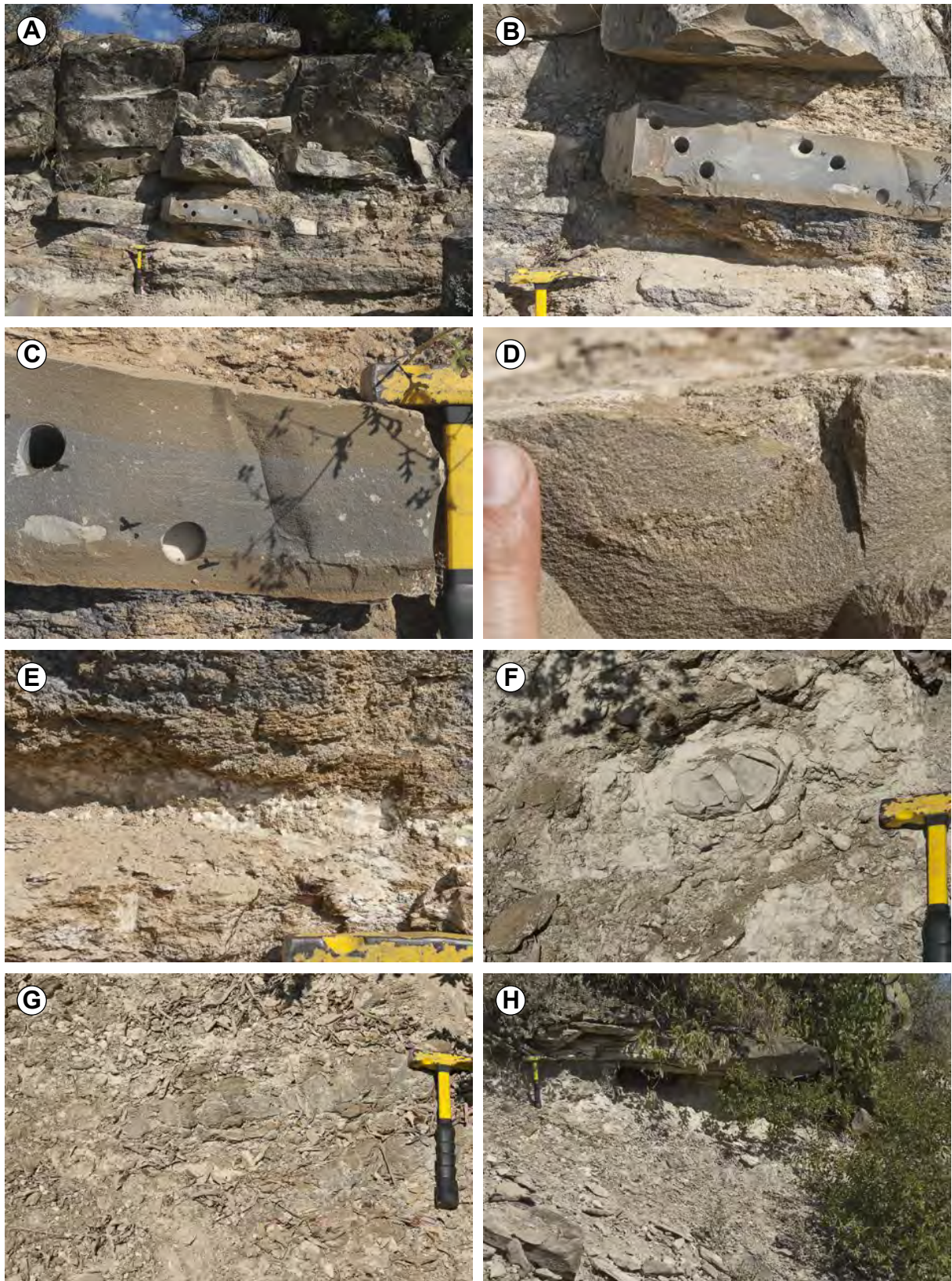
Figure S7: (caption on next page)

Figure S7 (page 11): Outcrop photos of the clastic unit and the disturbed Chicxulub ejecta deposit in the La Sierrita area (for additional details see *S28, S29*). (**A**) Succession of hills showing from right to left the Loma and the two Loma Cerca hills with the K-Pg clastic unit on top. (**B**) View on the Northern Loma Cerca showing the excellent exposures of the upper Maastrichtian marls along the flanks of the hills. No evidence for multiple laterally continuos "layers" of ejecta spherules is present. (**C**) Clastic deposit on top of the Loma Cerca. (**D** to **G**) Large "blobs" of slump folds and marl-spherule mixtures that are irregularly exposed for a few centimeters to several meters along the south-western flank of the Loma Cerca indicating pervasive soft-sediment deformation. (**H**) Thin red siltstone layers that are intercalated within the upper Maastrichtian marls below the spherule deposit. Their strike and dip (125°/40°) is clearly different from the nearly horizontally-lying clastic unit and indicates remobilization of upper Maastrichtian Méndez marls before deposition of the clastic unit. Hammer for scale (30 cm), top of hammer shows upsection.

Figure S8 (caption on next page).

Figure S8 (page 13): Outcrop photos of the clastic unit and the disturbed ejecta deposit in the El Peñón area. (**A**) Clastic deposit in the main quarry section. Note different dip directions of the lower part compared to the upper part of the section; hammer marks the base of the clastic deposit. (**B**) Detail of the basal part of the clastic deposit showing the spherule layer intercalated by a 10 cm-thick calcareous sandstone layer. (**C**) Detail of the calcareous sandstone showing large rip-up clasts at the base and faint lamination in the upper part. (**D**) The famous single J-shaped structure in the calcareous sandstone layer that was interpreted by Keller et al. (*S32*) as a burrow and as evidence for long-term deposition. However, besides this single structure at El Peñón, no evidence for bioturbation was observed in the up to 10 m thick, massive sands of the clastic unit in the outcrops of the La Popa, Rancho Nuevo, La Sierrita, El Mulato, La Lajilla, El Mimbral, or La Ceiba area (Figs. S6 to S8) (*S27, S30, S33*). Obviously, the presence of tracemakers is an extremely rare phenomenon in the northeastern Mexican clastic unit and confined to the top of the clastic unit. (**E**) Base of the spherule deposit with intercalated 3-cm thick layer of accretionary calcite spherules. (**F** and **G**) Slumped spherule deposit with large marl clasts about 200 m to the southeast of the main quarry outcrop showing doubling of spherule layer and mixing with upper Maastrichtian marls. (**H**) About 400 m from the main quarry outcrop to the southeast, the spherule deposit is again overlain by sandstone from the clastic unit (additional details in *S27*).
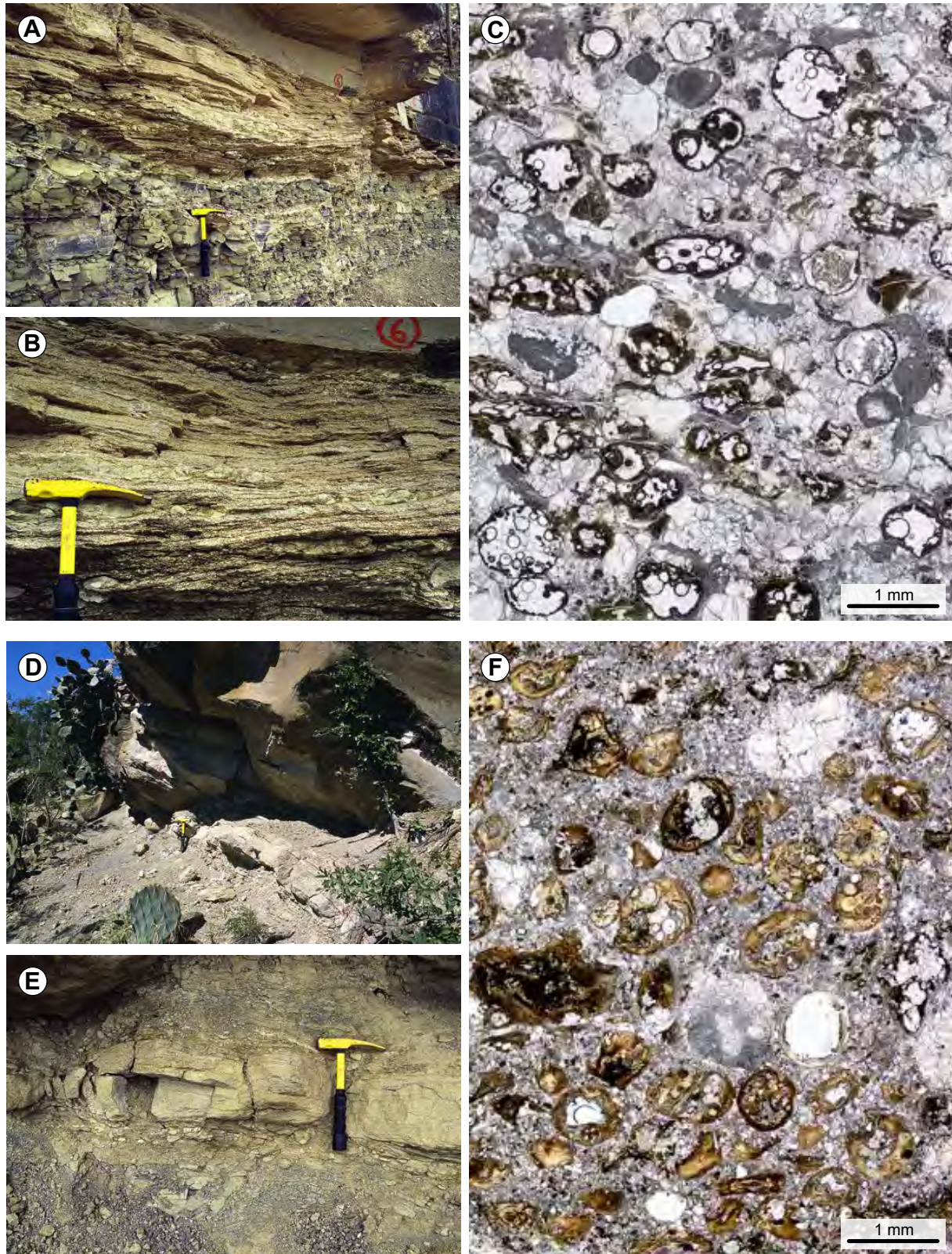
Figure S9 (caption on next page).

Figure S9 (page 15): Outcrop and corresponding thin-section photos of the basal ejecta bed of the clastic unit in northeastern Mexico. (**A**) Spherule deposit at El Mimbral at meter-mark 6. Note through-like wavy upper surface of the Méndez marls and presence of thin bentonite layer (at top of the hammer) below the laminated spherule bed similar to yellow clay layer the Cottonmouth Creek, Brazos (see Fig. S11). (**B**) Graded and laminated spherule deposit at El Mimbral. Note coarse, cm-sized ejecta (spherules and carbonate clasts), as well as marl clasts at the base. (**C**) Photomicrograph showing abundant spherules, limestone clasts, and blocky carbonate. (**D)** Spherule deposit at the Mesa Juan Perez 1A section showing alternating layers of weathered marl and spherule layers under- and overlying the indurated calcareous spherule layer. (**F**) Close-up of the laminated spherule layers showing alternating white layers of carbonaceous and spherule-rich ejecta. (**G**) Photomicrograph showing ejecta spherules, carbonate clasts, and minor fine-grained terrigeneous debris (e.g., quartz, feldspar). The presence of delicate petrographical structures, the compositional complexity of the deposit, and the absence of abrasion features or sorting suggests that this is a primary deposit with only minor transport at the seafloor.
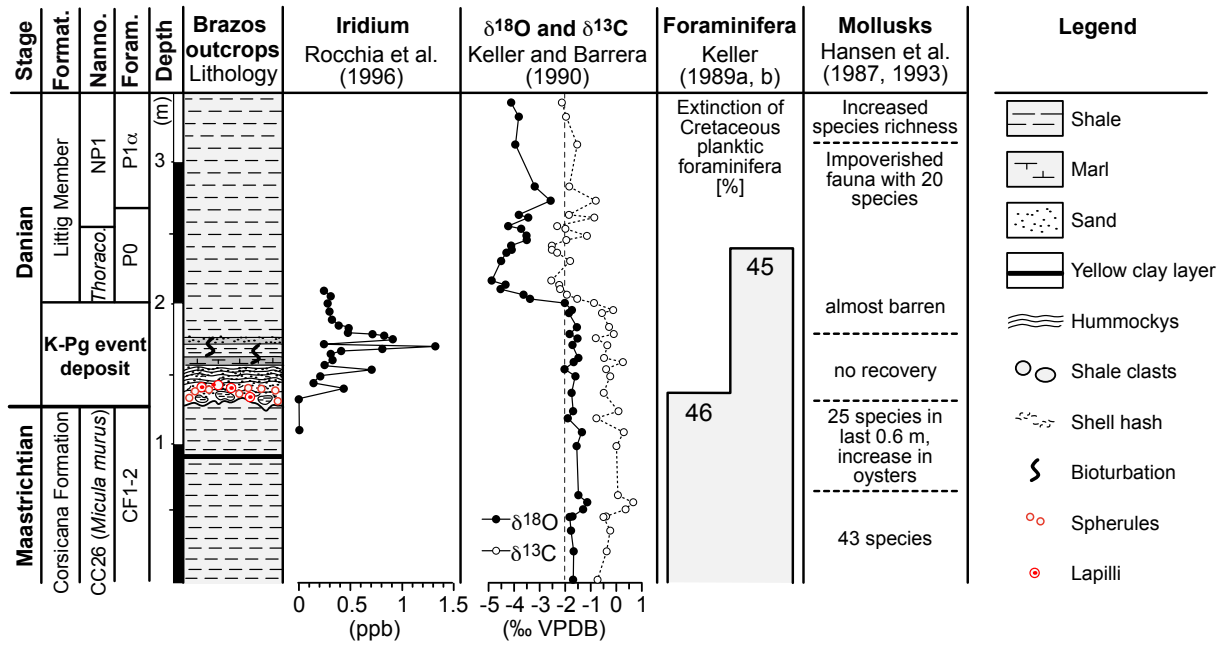
Figure S10: The K-Pg boundary in the Cottonmouth Creek, Brazos. A similar iridium distribution has been reported by Hansen et al. (*S34*) and Heyman et al. (*S35*).
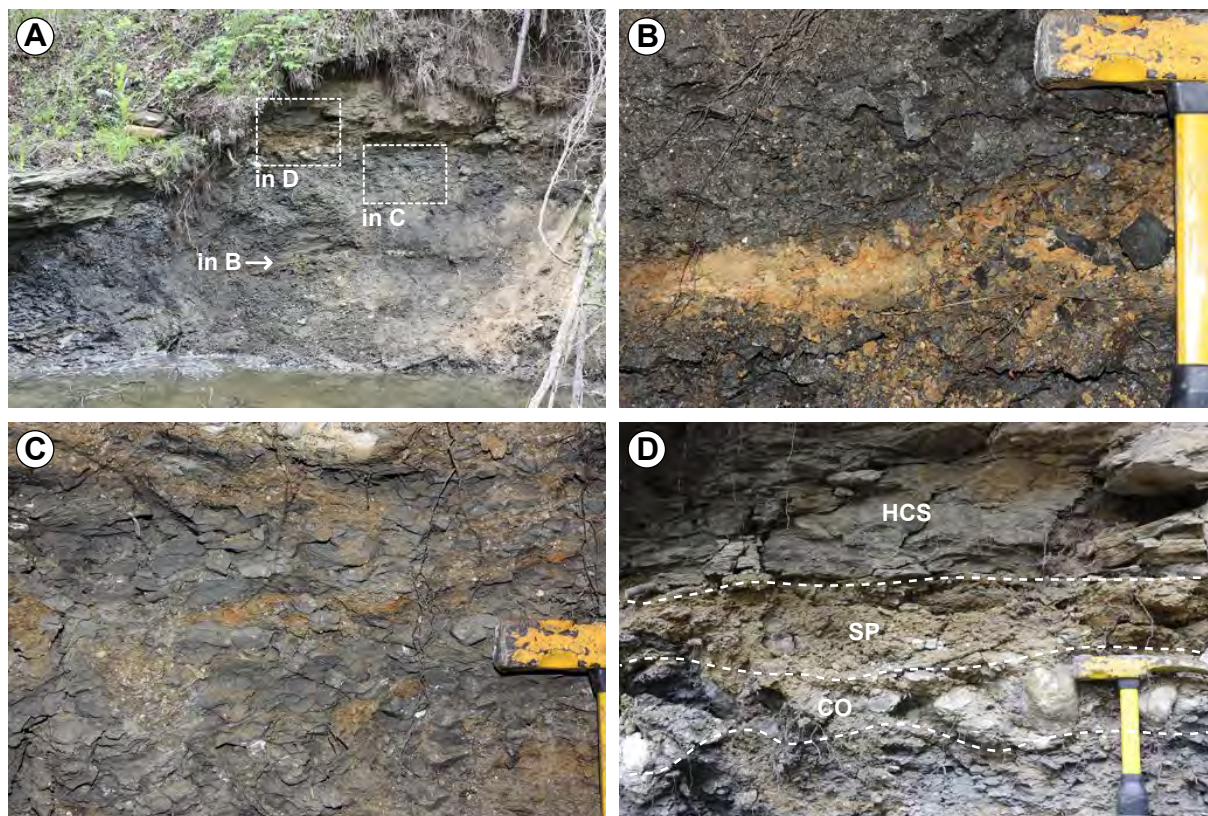
Figure S11: The K-Pg boundary at Brazos, Texas. (**A**) Overview of the K-Pg boundary interval at the Cottonmouth Creek, Brazos. (**B**) The upper Maastrichtian yellow clay layer was considered by Keller et al. (*S36*) as original Chicxulub ejecta. Our petrographical and mineralogical analysis – showing high quartz and sanidine contents – clearly contrasts with data for the Chicxulub ejecta layer (Table S3 and Fig. S12) and strongly indicate a volcanic origin of this yellow clay layer. Similar thin ash layers have been observed in upper Maastrichtian sections in northeastern Mexico and Haiti (Fig. S9) (*S37, S38*). (**C**) Disturbed uppermost Maastrichtian shales with large shale clasts separated by reddish, shell-rich clasts. (**D**) The K-Pg boundary event deposit consisting of a normally-graded, basal conglomeratic layer ("CO") with ejecta spherules, concretions, and shell hash, overlain by the spherule deposit ("SP") followed sequentially upward by repeated upward fining units of hummocky cross-bedded and laminated silicic and calcareous sands ("HCS"), which are burrowed in their uppermost parts, and then by a upward-fining silty shale unit (Fig. S7) (*S34, S35*, S39-*S41*). The K-Pg boundary is placed at the base of the ejecta-rich clastic unit (e.g., *S30*, *S41-S43*).
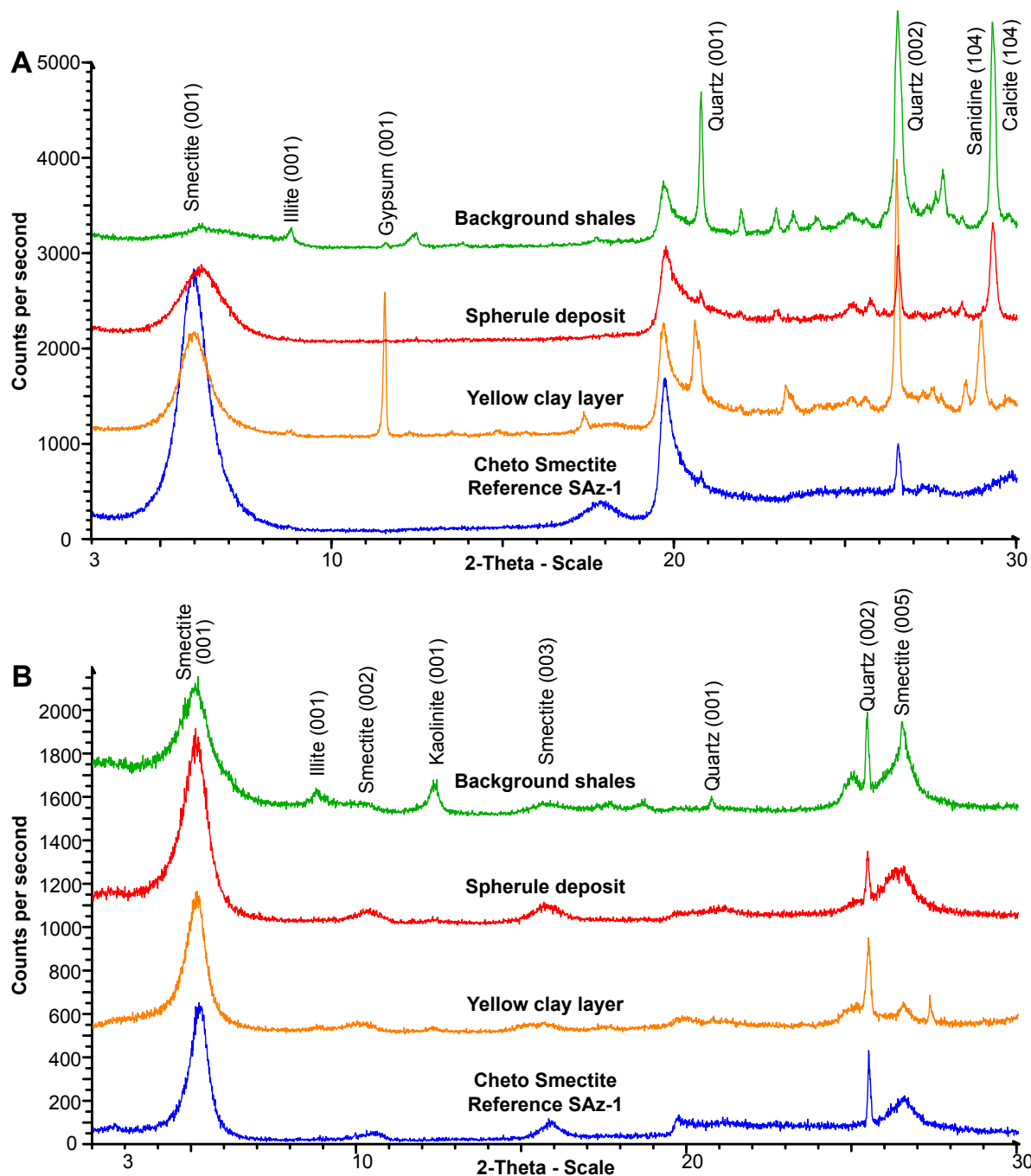
Figure S12: Mineralogy of the Brazos K-Pg section. (**A**) Bulk rock mineralogy and (**B**) clay mineralogy of the K-Pg boundary ejecta bed, the upper Maastrichtian yellow clay layer, and the background shales from the Cottonmouth Creek K-Pg section, Brazos, compared to the Cheto smectite from Arizona as reference (source clay SAz-2 as provided by the Clay Minerals Society, *S44*). Note differences in XRD patterns and specifically the high sanidine content of the yellow clay layer and absence of calcite, strongly suggesting a volcanic origin.
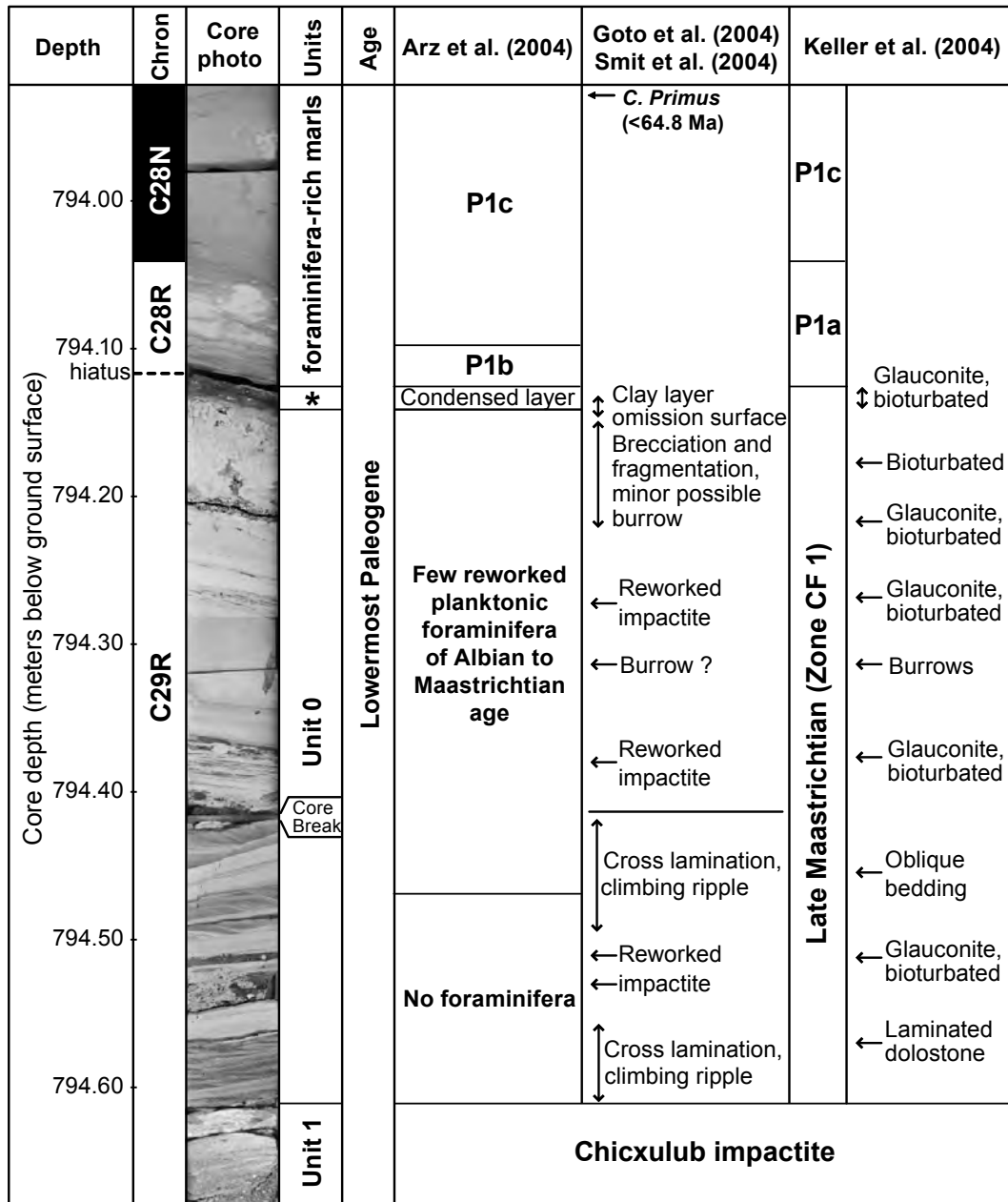
* dark clay layer

Figure S13: K-Pg boundary in core Yaxcopoil-1 – Photograph of the transition from the Chicxulub impact breccia to the lower Paleocene (modified after *S45*) showing observations from Goto et al. (*S46*), Arz et al., (*S47*), and Smit et al. (*S48*) versus Keller et al. (*S49*). The magnetostratigraphy is from Rebolledo-Vieyra and Urrutia-Fucugauchi (*S50*). Note that a distinct K-Pg boundary red clay layer (i.e., with an Ir anomaly, shocked minerals etc.) is lacking. Arz et al. (*S47*), Goto et al. (*S46*), and Smit et al. (*S48*) located the K-Pg boundary at the base of the impact sequence (at 894,94 m in core depth), according to the original definition of this boundary in the El Kef section, Tunisia (*S2*).
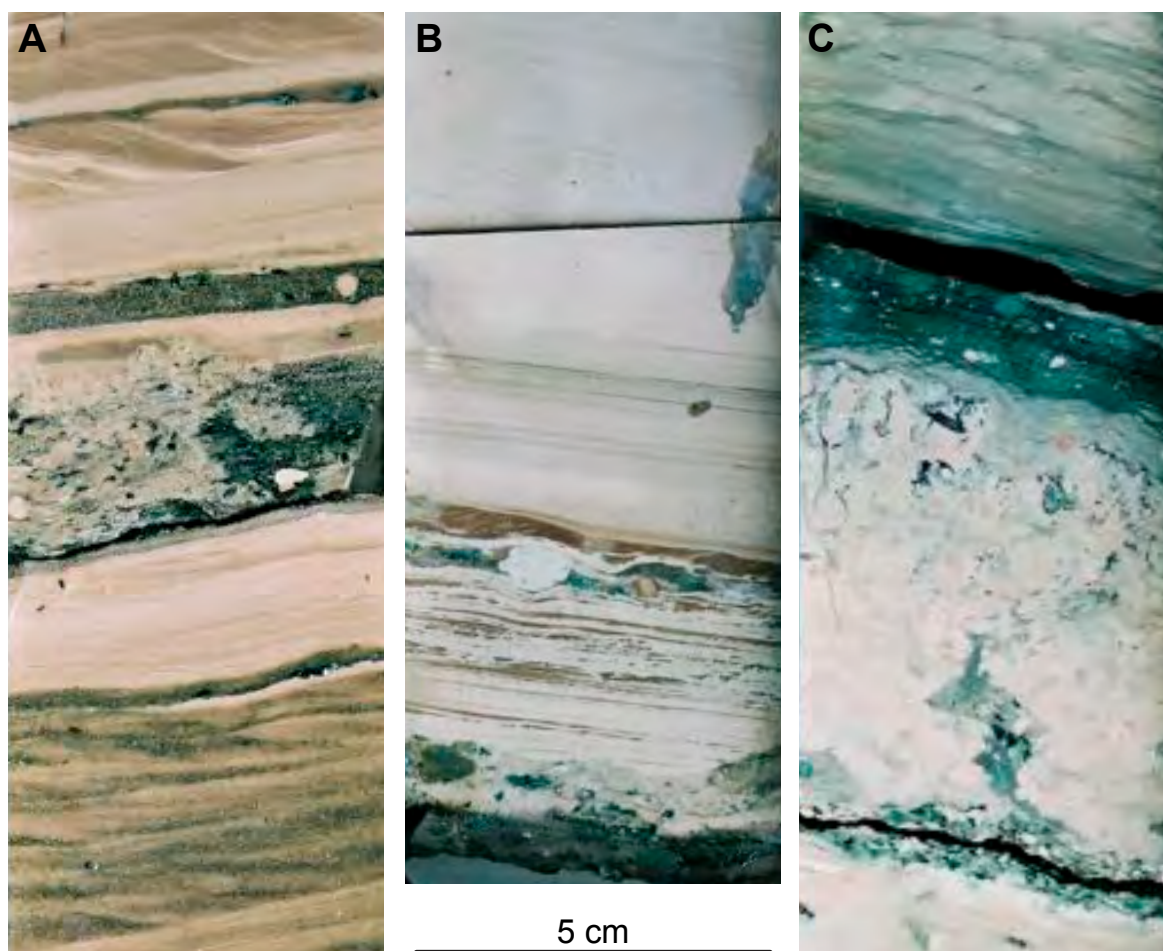
Figure S14: K-Pg boundary in core Yaxcopoil-1 – Close up photographs from (**A**) the lower part of unit 0 showing climbing ripples and cm-thick layers of ejecta-rich material, (**B**) the middle part of unit 0 with lamination and intercalated layers of ejecta-rich material; note that there is no bioturbation in the greenish sandstone layer, only the tube-like structure to the upper right may be a burrow (**C**) the condensed clay layer that overlies the uppermost part of unit 0 with an irregular erosion surface (modified after *S45*).
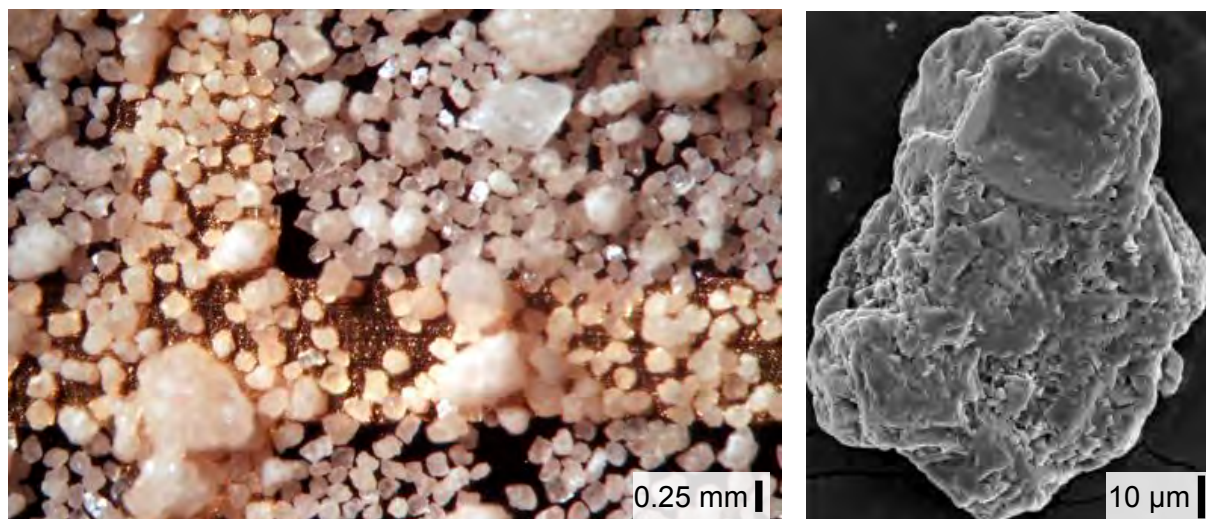
Figure S15: K-Pg boundary in core Yaxcopoil-1 – (**A**) Photographs of the washed residue showing abundant dolomite crystals as well as amalgamated dolomite crystals in a sample from the 794.55 m in core depth. This sample is equivalent to the sample Yax-20 of Keller et al. (*S49*) in which they allegedly identified the greatest planktonic foraminiferal diversity. (**B**) Scanning electron microscope image of an amalgamated dolomite clast that superficially resembles a planktonic foraminifer (at 794.55 m in core depth).
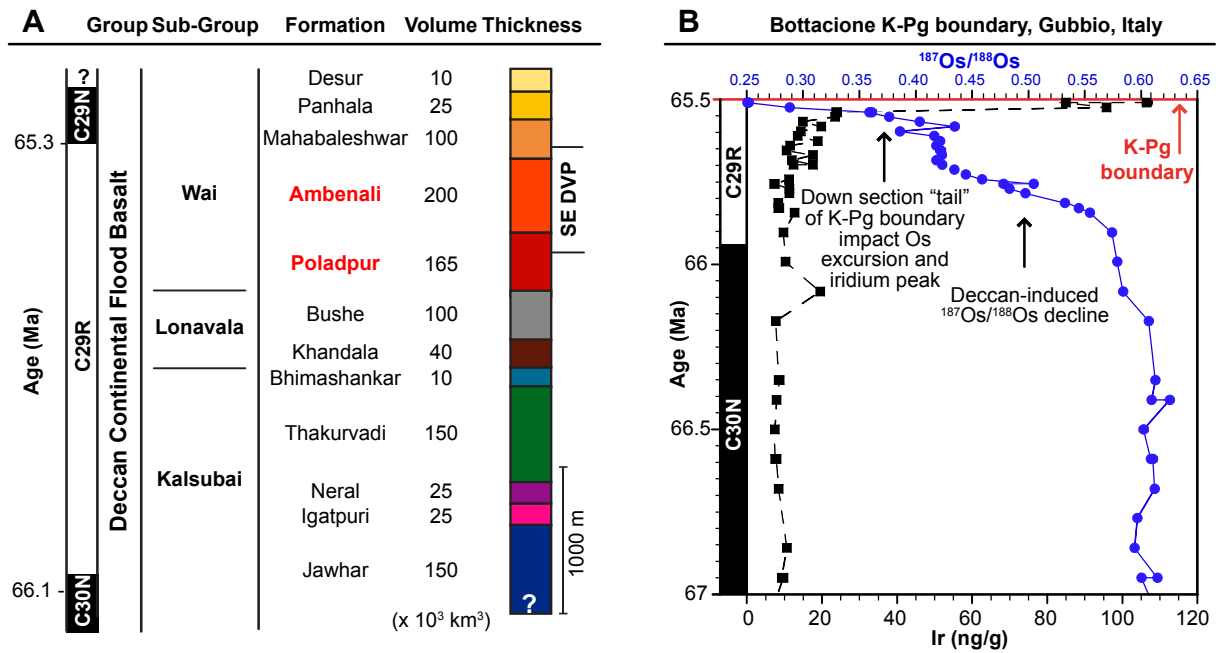
Figure S16: Compilation of the stratigraphic data for the emplacement phases of the Deccan flood basalts in southwest India. (**A**) Overview on stratigraphy, thickness, and volume of the lava flows (e.g., *S51*). Because the C29r/C29n reversal occurs in the lower Mahabaleshwar, the K-Pg boundary is most likely likely within the Poladpur and Ambenali formations marked in red, although the exact stratigraphic position has not been determined. (**B**) Os isotope data that are interpreted to show the onset of massive Deccan volcanism during the lower part of magnetochron C29r (*S22*).
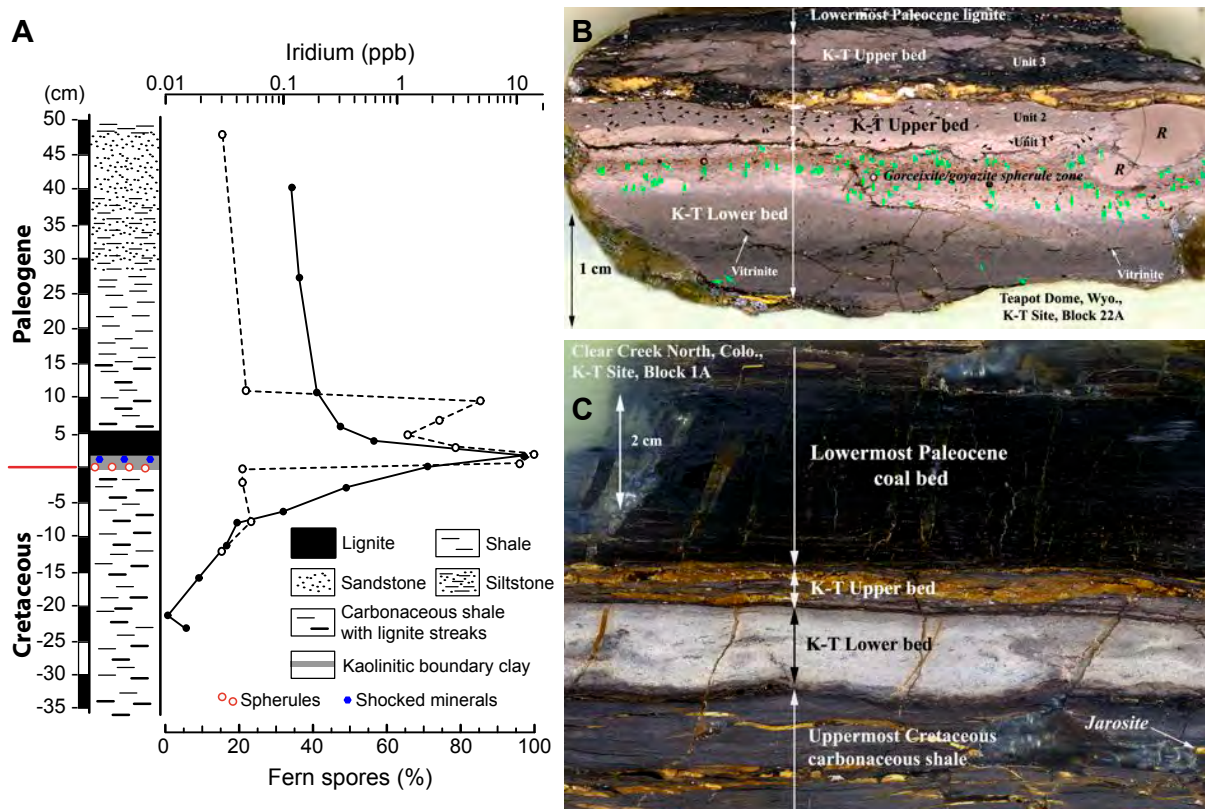
Figure S17: The K-Pg boundary in the Western Interior. (**A**) Schematic lithology of the K-Pg boundary interval at the Starkville North site, 5 km south of Trinidad, Colorado. The large black dots and the solid line show the iridium concentration, the open circles and the dashed line show the fern spore percentages (modified after *S52*). (**B**) Polished surface of the dual-layer K-Pg boundary claystone at the Teapot Dome site, Wyoming. Green arrows show ejecta spherules that are now altered to alumino-phosphate (gorceixite, goyzite) in the lower claystone. Black arrows show detrital quartz (shocked and unshocked) that is abundant in the upper claystone. Two large rip-up claystone clasts are marked with "R". Photo courtesy of Glen A. Izett. (**C**) Polished surface of the K-Pg boundary interval at the Clear Creek North site, Colorado. The lower K-Pg claystone bed consists of kaolinite clay and minor amounts of illite-smectite (I-S) mixed-layer phyllosilicates. Typically, this bed contains shreds and deformed laminae of vitrinite. This bed also contains ejecta spherules altered to kaolinite and alumino-phosphate. The upper part of the K-Pg claystone couplet is again compositionally and texturally different from the lower bed. It consists predominantly of illite-smectite (I-S) mixed-layer phyllosilicates and minor kaolinite and contains an assemblage of detrital silicate mineral grains (shocked and unshocked). Highest concentrations of the platinum group elements (PGEs) are usually present in the upper layer. Photo courtesy of Glen A. Izett.

Table S1: Key locations that show a detailed and expanded record across the K-Pg boundary including evidence for the presence of impact ejecta. See Fig. 1 for location of DSDP and ODP sites; color code for comparison with Fig. 2.

Region and K-Pg boundary sites	Distance*	Impact ejecta**	Max. Iridium concentration	Setting***	References
	(km)		(ppb)		
Very proximal to Chicxulub: 10 to >80 m-thick K-Pg boundary event deposit					
Southern Mexico and Cuba					
Guayal, Tabasco	300	SP, SQ, NI	0.8	Bathyal	(*S53-S55*)
Bochil, Chiapas	300	SP, SQ, NI	1.5	Bathyal	(*S6, S53-S55*)
Albion Island, Belize	300	SP, SQ	n.a.	Terrestrial	(*S56-S58*)
Moncada, Cuba	400	SP, SQ	0.5	Bathyal	(*S59*)
Loma Capiro, Santa Isabel, Peñalver, Cacarajícara, and Cidra, Cuba	400	SP, SQ	n.a.	Bathyal	(*S59-S62*)
Proximal to Chicxulub: dm to 10 m-thick K-Pg boundary event deposit					
Gulf of Mexico					
Beloc, Haiti	500	SP, SQ, NI	28	Bathyal	(*S63-S65*)
La Ceiba, Mexico	700	SP, SQ, NI	n.a.	Lower bathyal	(*S30, S33, S66*)
El Mimbral, Mexico	700	SP, SQ, NI	0.5	Lower bathyal	(*S27, S30, S66*)
La Lajilla, Mexico	750	SP, AC	0.25	Lower bathyal	(*S30, S66*)
El Mulato, Mexico	780	SP, AC	1	Lower bathyal	(*S6, S30*)
El Peñón, Mexico	800	SP, AC	n.a.	Middle bathyal	(*S27, S30, S66*)
La Sierrita, Mexico	800	SP, AC	0.3	Middle bathyal	(*S27, S28, S66*)
La Popa Basin, Mexico	800	SP, AC	n.a.	Inner neritic	(*S26, S67*)
Brazos River, Texas	900	SP, AC	n.a.	Neritic	(*S17, S30, S41, S43*)
Stoddard County, Missouri	900	SP	n.a.	Neritic	(*S68*)
Mussel Creek, Shell Creek, Antioch Church Core, Millers Ferry, Alabama	900	SP, AC	n.a.	Neritic	(*S25, S30, S69*)
Caribbean Sea					
ODP Leg 165: Site 999 and 1001	600	SP	n.a.	Bathyal	(*S70*)
Intermediate to Chicxulub: 1 to 10 cm-thick K-Pg boundary event deposit					
Western Interior (USA and Canada)					
Sugarite, Raton Basin, New Mexico	2100	SP, SQ (FS)	2.7	Terrestrial	(*S71-S73*)
Starkville South, Raton Basin, Colorado	2250	SP, SQ (FS)	56	Terrestrial	(*S71-S73*)
Starkville North, Raton Basin, Colorado	2250	SP, SQ (FS)	6	Terrestrial	(*S71-S73*)

Region and K-Pg boundary sites	Distance*	Impact ejecta**	Max. Iridium concentration	Setting***	References
	(km)		(ppb)		
Long Canyon, Raton Basin, Colorado	2250	SQ (FS)	8.2	Terrestrial	(S73, S74)
Berwind Canyon, Raton Basin, Colorado	2250	SP, SQ (FS)	27	Terrestrial	(S72, S73, S75)
West Bijou Site, Denver Basin, Colorado	2250	SQ (FS)	0.68	Terrestrial	(S73, S76)
Dogie Creek, Powder River Basin, Wyoming	2500	SP, SQ (FS)	20.8	Terrestrial	(S73, S77)
Teapot Dome, Powder River Basin, Wyoming	2500	SP, SQ (FS)	22	Terrestrial	(S73, S78)
Sussex, Powder River Basin, Wyoming	2500	SQ (FS)	26	Terrestrial	(S73, S79)
Mud Buttes, Williston Basin, SW North Dakota	2700	SP, SQ (FS)	1.36	Terrestrial	(S73, S80)
Brownie Butte, Hell Creek area, Montana	3100	SP, SQ (FS)	1.04	Terrestrial	(S52, S73, S81, S82)
Knudsen's Farm, Western Canada	3400	SQ (FS)	3.4	Terrestrial	(S73, S83)
Morgan Creek, Saskatchewan, Western Canada	3400	SQ (FS)	3	Terrestrial	(S73, S84)
Frenchman River, Saskatchewan	3400	SP	1.35	Terrestrial	(S72, S85)
Northwest Atlantic Ocean					
DSDP Leg 93 Site 603	2600	SP, SQ	n.a.	Bathyal	(S72, S86, S87)
ODP Leg 171 Site 1049, 1050, 1052	2400	SP, SQ	1.3	Lower bathyal	(S88)
ODP Leg 174AX Bass River	2500	SP, SQ, AC	n.a.	Neritic	(S89)
ODP Leg 207 Site 1258; 1259, 1260	4500	SP, SQ, AC	1.5	Bathyal	(S16, S90, S91)
<mark>**Distal to Chicxulub: mm-thick K-Pg boundary event deposit**</mark>					
South Atlantic Ocean					
DSDP Leg 75 Site 524	9600	n.a.	3	Abyssal	(S92)
ODP Leg 113 Site 690	11000	n.a.	1.5	Abyssal	(S93, S94)
ODP Leg 208 Site 1262, 1267	9400	SP, SQ	n.a.	Abyssal	(S90, S95)
Europe, Africa, Asia					
Gubbio and Petriccio, Italy	9200	SP, SQ, NI	8	Bathyal	(S96, S97)
Stevns Klint and Nye Kløv, Denmark	10200	SP, SQ, NI	48	Neritic	(S97-S101)
Bidart, France	9500	NI	6	Upper-middle bathyal	(S6, S102-S104)

Region and K-Pg boundary sites	Distance*	Impact ejecta**	Max. Iridium concentration	Setting***	References
	(km)		(ppb)		
Caravaca, Spain	8200	SP, SQ, NI	56	Bathyal	(*S6, S105-S107*)
Agost, Spain	8300	SP, SQ, NI	24.4	Upper-middle bathyal	(*S105, S108-S110*)
Bjala, Bulgaria	9500	SP, SQ, NI	6.1	Bathyal	(*S111*)
El Kef, Ellés, Tunisia	9100	SP, NI	18	Outer neritic – upper bathyal	(*S2, S6, S23*)
Aïn Settara, Tunisia	9100	SP, SQ, NI	11	Outer neritic – upper bathyal	(*S6, S112, S113*)
Pacific Ocean					
LL44-GPC 3	7200	SP, SQ, NI	12	Abyssal	(*S114*)
DSDP Leg 62 Site 465	7900	SP, SQ, NI	54	Lower bathyal	(*S114-S117*)
DSDP Leg 86 Site 576, 577	9300	SP, SQ, NI	13.4	Abyssal	(*S114, S118, S119*)
DSDP Leg 91 Site 596	9700	SP, SQ, NI	10.8	Abyssal	(*S120*)
ODP Leg 119 Site 738	10500	–	18	Abyssal	(*S121-S123*)
ODP Leg 130 Site 803, 807	11000	SP, SQ, NI	10.8	Abyssal	(*S114, S124*)
ODP Leg 145 Site 886	6450	SP, SQ, NI	3.6	Abyssal	(*S114, S125*)
ODP Leg 198 Site 1209 to 1212	11400	–	n.a.	Abyssal	(*S43, S126*)
Woodside Creek, New Zealand	10500	SP, SQ, NI (FS)	70	Bathyal	(*S14, S90, S127, S128*)
Mid-Waipara, New Zealand	10500	SP (FS)	0.49	Neritic	(*S129-S134*)
Flaxbourne River, New Zealand	10500	SP	21	Upper-middle bathyal	(*S14, S135*)
Moody Creek Mine, New Zealand	10500	SP (FS)	4.1	Terrestrial	(*S136*)

* Estimated paleodistance to the center of the Chicxulub crater structure.

** SP, spherules; SQ, shocked quartz; NI, Ni-rich spinel; (FS), fern spore spike.

*** We used the bathymetric division as defined in Van Morkhoven et al. (*S137*): neritic (0-200 m), upper bathyal (200-600 m), middle bathyal (600-1000 m), lower bathyal (1000-2000 m), upper abyssal (2000-3000 m), lower abyssal (>3000 m).

Table S2: Compilation of U-Pb ages from zircons from the Chicxulub impact crater, various K-Pg boundary sites, and the potential basement of the Yucatán target region (Maya Mountains, Belize).

Locality	Material	Basement age (Ma) ± 2σ*	Method	References
Chicxulub crater impactites; spherule deposit Beloc, Haiti; laminated clay layer at K-Pg boundary in Colorado	Shocked zircons	545 ± 5; 418 ± 6	U-Pb	(*S10*)
Laminated clay layer at K-Pg boundary, Colorado	Shocked zircons	550 ± 10; 571 ± 6	U-Pb	(*S138*, *S139*)
Laminated clay layer at K-Pg boundary, Saskatchewan	Shocked zircons	548 ± 8	U-Pb	(*S140*)
Silurian plutons, Maja Mountains	Zircons	418 ± 4; 404 ± 3	U-Pb	(*S141*)
Paleozoic granite	Zircons	595 ± 69; 680 ± 69	U-Pb	(*S142*)

* number refers to the last significant digits

Table S3: Quantitative mineralogy of the K-Pg boundary ejecta bed, the upper Maastrichtian ash layer, the background shales and a reference Cheto smectite from Arizona.

Mineral phases (wt%)	Cheto smectite Reference clay SAz-1	Yellow ash layer	Spherule deposit	Background shales
Quartz	1.2	5.5	1.9	17.4
Orthoclase	<0.1	0.4	0.5	1.4
Microcline	0.7	0.5	1.3	1.3
Plagioclase	9	1.6	5.7	5.5
Anorthite	0.2	0.9	0.2	0.8
Sanidine	1	3.5	<0.1	1.9
Calcite	0.6	2.2	5	7.5
Dolomite	<0.1	<0.1	0.2	0.2
Smectite	81.8	63.5	74.8	28.1
Illite1Md	4.8	13.9	5.3	28.8
Kaolinite	<0.1	1.3	2	5.4
Gypsum	0.2	4.6	0.7	0.3
Pyrite	<0.1	0.2	2.1	1.1
Goethite	<0.1	0.4	0.6	<0.1
Jarosite	0.7	1.6	<0.1	0.2

Supporting References

S1.   J. Srodon, V. A. Drits, D. K. McCarty, J. C. C. Hsieh, D. D. Eberl, *Clays Clay Miner.* **49**, 514 (2001).

S2.   E. Molina *et al.*, *Episodes* **29**, 263 (2006).

S3.   J. J. Pospichal, *Geology* **22**, 99 (1994).

S4.   S. Gardin, S. Monechi, *Bulletin de la Société Géologique de France* **169**, 709 (1998).

S5.   I. Arenillas, J. A. Arz, E. Molina, C. Dupuis, *Micropaleontology* **46**, 31 (2000).

S6.   E. Molina *et al.*, *Episodes* **32**, 84 (2009).

S7.   W. C. Ward, G. Keller, W. Stinnesbeck, T. Adatte, *Geology* **23**, 873 (1995).

S8.   B. Kettrup, A. Deutsch, *Meteor. Planet. Sci.* **38**, 1079 (2003).

S9.   S. P. S. Gulick *et al.*, *Nature Geosci.* **1**, 131 (2008).

S10.   T. E. Krogh, S. L. Kamo, V. L. Sharpton, L. E. Marin, A. R. Hildebrand, *Nature* **366**, 731 (1993).

S11.   V. L. Sharpton, B. C. Schuraytz, K. Burke, A. V. Murali, G. Ryder, *Geol. Soc. Am. Spec. Pap.* **247**, 349 (1990).

S12.   R. D. Norris, B. T. Huber, B. T. Self-Trail, *Geology* **27**, 419 (1999).

S13.   B. Bauluz, D. R. Peacor, W. C. Elliott, *Earth Planet. Sci. Lett.* **182**, 127 (2000).

S14.   B. Bauluz, D. R. Peacor, C. J. Hollis, *Earth Planet. Sci. Lett.* **219**, 209 (2004).

S15.   M. Ortega-Huertas, F. Martínez-Ruiz, I. Palomo-Delgado, H. Chamley, *Clay Minerals* **37**, 395 (2002).

S16.   P. Schulte *et al.*, Geochim. Cosmochim. Acta **73**, 1180 (2009).

S17.   T. E. Yancey, R. N. Guillemette, *Geol. Soc. Am. Bull.* **120**, 1105 (2008).

S18.   M. C. Harvey, S. C. Brassell, C. M. Belcher, A. Montanari, *Geology* **36**, 355 (2008).

S19.   C. M. Belcher, P. Finch, M. E. Collinson, A. C. Scott, N. V. Grassineau, *Proc. Nat. Acad. Sci.* **106**, 4112 (2009).

S20.   K. F. Kuiper *et al.*, *Science* **320**, 500 (2008).

S21.   W. Alvarez, F. Asaro, A. Montanari, *Science* **250**, 1700 (1990).

S22.   N. Robinson, G. Ravizza, R. Coccioni, B. Peucker-Ehrenbrink, R. D. Norris, *Earth Planet. Sci. Lett.* **281**, 159 (2009).

S23.   G. Keller, M. Lindinger, Palaeogeogr. Palaeoclimatol. Palaeoecol. **73**, 243 (1989).

S24.   R. Rocchia, E. Robin, L. Froget, J. Gayraud, *Geol. Soc. Am. Spec. Paper* **307**, 279 (1996).

S25.   D. T. King,Jr., L. W. Petruny, *Geol. Soc. Am. Spec. Pap.* **437**, 179 (2007).

S26.   T. F. Lawton, K. W. Shipley, J. L. Aschoff, K. A. Giles, F. J. Vega, *Geology* **33**, 81 (2005).

S27.   P. Schulte, A. Kontny, *Geol. Soc. Am. Spec. Pap.* **384**, 191 (2005).

S28.   A. R. Soria *et al.*, *Geology* **29**, 231 (2001).

S29.   P. Schulte *et al.*, *Intern. Jour. Earth Sci.* **92**, 114 (2003).

S30.   J. Smit, W. Alvarez, A. Montanari, P. Claeys, J. M. Grajales-Nishimura, *Geol. Soc. Am. Spec. Paper* **307**, 151 (1996).

S31.   F. Lindenmaier *et al.*, *Chemostratigraphy of the K/T-boundary at La Sierrita and La Lajilla, NE Mexico*. (Abstracts, Geol. Soc. Am., Boulder, Colorado, 1999), pp. 123.

S32.   G. Keller, W. Stinnesbeck, T. Adatte, D. Stüben, *Earth-Sci. Rev.* **62**, 327 (2003).

S33.   J. A. Arz *et al.*, *J. South Am. Earth Sci.* **14**, 505 (2001).

S34.   T. A. Hansen, B. Upshaw III, E. G. Kauffman, W. Gose, *Cretaceous Res.* **14**, 685 (1993).

S35.   D. Heymann *et al.*, *Geochim. Cosmochim. Acta* **62**, 173 (1998).

S36.   G. Keller *et al.*, *Earth Planet. Sci. Lett.* **255**, 339 (2007).

S37.   J. Smit *et al.*, *Geology* **20**, 99 (1992).

S38.   D. A. Kring, A. R. Hildebrand, W. V. Boynton, *Earth Planet. Sci. Lett.* **128**, 629 (1994).

S39.   T. A. Hansen, R. B. Farrand, H. A. Montgomery, H. G. Billman, G. L. Blechschmidt, *Cretaceous Res.* **8**, 229 (1987).

S40.   T. E. Yancey, *Gulf Coast Association of Geological Societies Transactions* **46**, 433 (1996).

S41.   P. Schulte, R. P. Speijer, H. Mai, A. Kontny, *Sedim. Geol.* **184**, 77 (2006).

S42.   P. Schulte *et al.*, *Earth Planet. Sci. Lett.* **269**, 613 (2008).

S43.   T. J. Bralower *et al.*, *Geology* (in press) (2010).

S44.   S. J. Chipera, D. L. Bish, *Clays Clay Miner.* **49**, 308 (2001).

S45.   K. Goto, *Journal of the Geological Society of Japan* **111**, 193 (2005).

S46.   K. Goto *et al.*, *Meteor. Planet. Sci.* **39**, 1233 (2004).

S47.   J. A. Arz, L. Alegret, I. Arenillas, *Meteor. Planet. Sci.* **39**, 1099 (2004).

S48.   J. Smit, S. V. D. Gaast, W. Lustenhouwer, *Meteor. Planet. Sci.* **39**, 1113 (2004).

S49.   G. Keller *et al.*, *Meteor. Planet. Sci.* **39**, 1127 (2004).

S50.   M. Rebolledo-Vieyra, J. Urrutia-Fucugauchi, *Meteor. Planet. Sci.* **39**, 821 (2004).

S51.   S. Self, M. Widdowson, T. Thordarson, A. E. Jay, *Earth Planet. Sci. Lett.* **248**, 518 (2006).

S52.   R. H. Tschudy, C. L. Pillmore, C. J. Orth, J. S. Gilmore, J. D. Knight, *Science* **225**, 1030 (1984).

S53.   J. M. Grajales-Nishimura, G. Murillo-Muñetón, C. Rosales-Domínguez, E. Cedillo-Pardo, J. García-Hernández, *AAPG Mem.* **79**, 312 (2003).

S54.   I. Arenillas *et al.*, *Earth Planet. Sci. Lett.* **249**, 241 (2006).

S55.   T. Salge, *The ejecta blanket of the Chicxulub impact crater, Yucatán, Mexico – Petrographic and chemical studies of the K-P section of El Guayal and UNAM boreholes* (PhD, Humboldt-Universität, Berlin, Germany, 2007), pp. 190. http://edoc.hu-berlin.de/docviews/abstract.php?lang=ger&id=27753.

S56.   K. O. Pope *et al.*, *Earth Planet. Sci. Lett.* **170**, 351 (1999).

S57.   K. O. Pope *et al.*, *Geol. Soc. Am. Spec. Pap.* **384**, 171 (2005).

S58.   B. W. Fouke *et al.*, *Sedimentology* **49**, 117 (2002).

S59.   R. Tada *et al.*, *Geol. Soc. Am. Spec. Pap.* **356**, 109 (2002).

S60.   S. Kiyokawa *et al.*, *Geol. Soc. Am. Spec. Pap.* **356**, 125 (2002).

S61.   L. Alegret *et al.*, *Geology* **33**, 721 (2005).

S62. K. Goto *et al.*, *Cretaceous Res.* **29**, 217 (2008).

S63. G. A. Izett, *J. Geophys. Res.* **96**, 20879 (1991).

S64. H. Leroux *et al.*, *Earth Planet. Sci. Lett.* **131**, 255 (1995).

S65. B. F. Bohor, B. P. Glass, *Meteoritics* **30**, 182 (1995).

S66. L. Alegret, E. Molina, E. Thomas, *Geology* **29**, 891 (2001).

S67. J. L. Aschoff, K. A. Giles, *AAPG Bulletin* **89**, 447 (2005).

S68. C. E. Campbell, F. E. Oboh-Ikuenobe, T. L. Eifert, *Geol. Soc. Am. Spec. Pap.* **437**, 189 (2007).

S69. P. Schulte, R. Speijer, *Geologica Acta* **7**, 11 (2009).

S70. H. Sigurdsson, R. M. Leckie, G. D. Acton, *Proc. ODP Init. Rep.* **165**, 377 (1997).

S71. C. L. Pillmore, R. H. Tschudy, C. J. Orth, J. S. Gilmore, J. D. Knight, *Science* **223**, 1180 (1984).

S72. G. A. Izett, *Geol. Soc. Am. Spec. Paper* **249**, 100 (1990).

S73. D. J. Nichols, K. R. Johnson, *Plants and the K-T boundary* (Cambridge University Press, 2008), pp. 280.

S74. D. J. Nichols, C. L. Pillmore, *LPI Contribution* **38**, 3120 (2000).

S75. C. J. Orth, J. S. Gilmore, J. D. Knight, *New Mexico Geological Society Guidebook* **38**, 265 (1987).

S76. R. S. Barclay, K. R. Johnson, *Geol. Soc. Am. Field Guide* **5**, 59 (2004).

S77. B. F. Bohor, D. M. Triplehorn, D. J. Nichols, H. T. Millard,Jr., *Geology* **15**, 896 (1987).

S78. J. A. Wolfe, *Nature* **352**, 420 (1991).

S79. D. J. Nichols, J. L. Brown, M. Attrep,Jr., C. J. Orth, *Cretaceous Res.* **13**, 3 (1992).

S80. D. J. Nichols, K. R. Johnson, *Geol. Soc. Am. Spec. Paper* **361**, 95 (2002).

S81. B. F. Bohor, G. A. Izett, *Lunar Planet. Sci.* **17**, 68 (1986).

S82. A. R. Sweet, D. R. Braman, J. F. Lerbekmo, *Can. J. Earth Sci.* **36**, 743 (1999).

S83. A. R. Sweet, D. R. Braman, *Cretaceous Res.* **13**, 31 (1992).

S84. D. J. Nichols, D. M. Jarzen, C. J. Orth, P. Q. Oliver, *Science* **231**, 714 (1986).

S85. D. A. Kring, D. D. Durda, *J. Geophys. Res.* **107**, 6 (2002).

S86. G. T. Klaver, T. M. G. Van Kempen, F. R. Bianchi, *Initial Rep. Deep Sea Drill. Proj.* **93**, 1039 (1987).

S87. D. A. Kring, *J. Geophys. Res.* **100**, 16979 (1995).

S88. F. Martínez-Ruiz, M. Ortega-Huertas, I. Palomo-Delgado, J. Smit, *Geol. Soc. Am. Spec. Paper* **356**, 189 (2002).

S89. R. K. Olsson, K. G. Miller, J. V. Browning, D. Habib, P. J. Sugarmann, *Geology* **25**, 759 (1997).

S90. J. V. Morgan *et al.*, *Earth Planet. Sci. Lett.* **251**, 264 (2006).

S91. K. G. MacLeod, D. L. Whitney, B. T. Huber, C. Koeberl, *Geol. Soc. Am. Bull.* **119**, 101 (2007).

S92. K. J. Hsü *et al.*, *Science* **216**, 249 (1982).

S93. H. V. Michel, F. Asaro, W. Alvarez, L. W. Alvarez, *Sci. Res., Proc. Ocean Drill. Prog.* **113**, 159 (1990).

S94. L. D. Stott, J. P. Kennett, *Nature* **342**, 526 (1989).

S95. L. Alegret, E. Thomas, *Mar. Micropal.* **64**, 1 (2007).

S96. A. Montanari, *Jour. Sedim. Petrol.* **61**, 315 (1991).

S97. J. Smit, *Ann. Rev. Earth Planet. Sci.* **27**, 75 (1999).

S98. F. T. Kyte, Z. Zhou, J. T. Wasson, *Nature* **288**, 651 (1980).

S99. B. Schmitz, P. Andersson, J. Dahl, *Geochim. Cosmochim. Acta* **52**, 229 (1988).

S100. R. Frei, K. M. Frei, *Earth Planet. Sci. Lett.* **203**, 691 (2002).

S101. A. Trinquier, J.-L. Birck, C. J. Allègre, *Earth Planet. Sci. Lett.* **241**, 780 (2006).

S102. J. Smit, W. G. H. Z. ten Kate, *Cretaceous Res.* **3**, 307 (1982).

S103. L. Alegret, M. A. Kaminski, E. Molina, *Palaios* **19**, 574 (2004).

S104. N. Gallala, D. Zaghbib-Turki, I. Arenillas, J. A. Arz, E. Molina, *Mar. Micropal.* **72**, 196 (2009).

S105. F. Martínez-Ruiz, M. Ortega-Huertas, I. Palomo-Delgado, P. Acquafredda, *Sedim. Geol.* **113**, 137 (1997).

S106. K. Kaiho *et al.*, *Paleoceanography* **14**, 511 (1999).

S107. J. Smit, *Journal of Iberian Geology* **31**, 179 (2005).

S108. F. Martínez-Ruiz, M. Ortega-Huertas, I. Palomo-Delgado, M. Barbieri, *Chem. Geol.* **95**, 265 (1992).

S109. L. Alegret, E. Molina, E. Thomas, *Mar. Micropal.* **48**, 251 (2003).

S110. E. Molina, L. Alegret, I. Arenillas, J. A. Arz, *Journal of Iberian Geology* **31**, 137 (2004).

S111. A. Preisinger *et al.*, *Geol. Soc. Am. Spec. Pap.* **356**, 213 (2002).

S112. C. Dupuis *et al.*, *Bulletin de l'Institut Royal des Sciences Naturelles de Belgique, Sciences de la Terre* **71**, 169 (2001).

S113. D. Peryt, L. Alegret, E. Molina, *Terra Nova* **14**, 101 (2002).

S114. J. A. Bostwick, F. T. Kyte, *Geol. Soc. Am. Spec. Paper* **307**, 403 (1996).

S115. H. V. Michel, F. Asaro, W. Alvarez, L. W. Alvarez, *Initial Rep. Deep Sea Drill. Proj.* **62**, 847 (1981).

S116. P. Giblin, *Initial Rep. Deep Sea Drill. Proj.* **62**, 851 (1981).

S117. L. Alegret, E. Thomas, *Palaeogeogr. Palaeoclimatol. Palaeoecol.* **224**, 53 (2005).

S118. A. A. Wright *et al.*, *Initial Rep. Deep Sea Drill. Proj.* **86**, 799 (1985).

S119. H. V. Michel, F. Asaro, W. Alvarez, L. W. Alvarez, *Initial Rep. Deep Sea Drill. Proj.* **86**, 533 (1985).

S120. F. T. Kyte, J. A. Bostwick, L. Zhou, *Geol. Soc. Am. Spec. Pap.* **307**, 389 (1996).

S121. B. Schmitz, F. Asaro, H. V. Michel, H. R. Thierstein, B. T. Huber, *Sci. Res., Proc. Ocean Drill. Prog.* **119**, 719 (1991).

S122. B. T. Huber, *Sci. Res., Proc. Ocean Drill. Prog.* **119**, 451 (1991).

S123. A. Abrajevitch, K. Kodama, *Earth Planet. Sci. Lett.* **286**, 269 (2009).

S124. R. M. Corfield, J. E. Cartlidge, *Sci. Res., Proc. Ocean Drill. Prog.* **130**, 259 (1993).

S125. B. L. Ingram, *Sci. Res., Proc. Ocean Drill. Prog.* **145**, 399 (1995).

S126.   T. J. Bralower, I. Premoli Silva, M. J. Malone, *Sci. Res., Proc. Ocean Drill. Prog.* **198**, 1 (2006).

S127.   R. R. Brooks *et al.*, *Geology* **13**, 738 (1985).

S128.   R. R. Brooks *et al.*, *Science* **226**, 539 (1984).

S129.   R. R. Brooks *et al.*, *Geology* **14**, 727 (1986).

S130.   P. S. Willumsen, *GFF* **122**, 180 (2000).

S131.   P. S. Willumsen, *Journal of Micropalaeontology* **23**, 119 (2004).

S132.   P. S. Willumsen, *Alcheringa* (in press) (2010).

S133.   C. J. Hollis, C. P. Strong, *New Zealand Journal of Geology & Geophysics* **46**, 243 (2003).

S134.   V. Vajda, J. I. Raine, *New Zealand Journal of Geology & Geophysics* **46**, 255 (2003).

S135.   C. J. Hollis, C. P. Strong, K. A. Rodgers, K. M. Rogers, *New Zealand Journal of Geology & Geophysics* **46**, 177 (2003).

S136.   V. Vajda, J. I. Raine, C. J. Hollis, C. P. Strong, in *Global effects of the Chicxulub impact on terrestrial vegetation: Review of the palynological record from New Zealand Cretaceous/ Tertiary boundary*, H. Dypvik, M. J. Burchell, P. Claeys, Eds. (Springer, Berlin, Germany, 2004), pp. 57-74.

S137.   F. P. C. M. Van Morkhoven, B. W.A., S. A. Edwards, *Bull. Centr. Rech. Explor. - Production Elf-Aquitaine, Mémoir* **11**, 1 (1986).

S138.   T. E. Krogh, S. L. Kamo, B. F. Bohor, *Earth Planet. Sci. Lett.* **119**, 425 (1993).

S139.   W. R. Premo, G. A. Izett, G. P. Meeker, *Lunar Planet. Sci.* **26**, 1139 (1995).

S140.   S. L. Kamo, T. E. Krogh, *Geology* **23**, 281 (1995).

S141.   M. B. Steiner, J. D. Walker, *J. Geophys. Res.* **101**, 17727 (1996).

S142.   R. Lopez, K. L. Cameron, N. W. Jones, *Precambrian Res.* **107**, 195 (2001).